International Journal of Disaster Risk Reduction 128 (2025) 105746

Contents lists available at ScienceDirect

International Journal of Disaster Risk Reduction

journal homepage: www.elsevier.com/locate/ijdrr

Resilience Readiness Levels for buildings: Establishing multi-hazard resilience metrics and rating systems

Simona Bianchi [a,*], Michele Matteoni [b], Kyujin Kim [a], Anna Maria Koniari [a], Kyra Koning [c], Romulus Costache [d], Nicu Ciobotaru [d], Alessandra Luna-Navarro [a], Zhikai Peng [a,c], Jonathan Ciurlanti [e], Hamidreza Shahriari [f], Divyae Mittal [f], Evdokia Stavridou [f], Anna Silva [a,c], Michele Palmieri [e], Stefano Pampanin [b], Francesco Petrini [b], Mauro Overend [a]

[a] Delft University of Technology, 2628 BL, Delft, the Kingdom of the Netherlands
[b] Sapienza University of Rome, 00184, Rome, Italy
[c] Amsterdam Institute for Advanced Metropolitan Solutions, 1018 JA, Amsterdam, the Kingdom of the Netherlands
[d] Transilvania University of Brasov, 500123, Brasov, Romania
[e] Arup, 1043 CA, Amsterdam, the Kingdom of the Netherlands
[f] OMRT, 1013 AC, Amsterdam, the Kingdom of the Netherlands

ARTICLE INFO

Keywords:
Resilience
Buildings
Multi-hazard
Performance-based
Risk assessment
Decision making

ABSTRACT

The built environment is vulnerable to climate-induced extreme events and natural disasters, which are repeatedly exposing communities to severe consequences and market disruptions. In response, the construction industry is developing resilient technologies for buildings, but the proposed solutions are often not cost-effective, rarely eco-friendly and typically fail to address multiple hazards present in many locations. These shortcomings stem from the absence of a clearly defined framework for quantifying holistic multi-hazard resilience. As a result, investment decisions are ill-informed and technical solutions are sub-optimal. This paper redresses this issue by proposing quantitative indicators and introducing the Resilience Readiness Levels to assess the resilience of buildings, considering multi-domain factors (physical, social, economic, environmental) in single or multi-hazard contexts (heat, seismic, wind, flood). The proposed resilience indices and calculation methods are based on a diverse set of scientific literature and real-world practices, and are demonstrated on Dutch and Italian urban blocks with different local hazards and building layouts. The results show that the multi-domain resilience approach can support informed early-stage building design and retrofit decision-making for single hazards, while aiding prioritization and intervention planning for improving building disaster preparedness in multi-hazard scenarios.

1. Introduction

There is a pressing need for resilient communities. The devastating impacts of recent climatic events have triggered systemic failures across multiple sectors globally. In Europe alone, economic losses from climate-induced events amounted to €650 billion

* Corresponding author.
E-mail address: s.bianchi@tudelft.nl (S. Bianchi).

https://doi.org/10.1016/j.ijdrr.2025.105746
Received 10 March 2025; Received in revised form 5 August 2025; Accepted 6 August 2025
Available online 7 August 2025

between 1980 and 2022, of which only one third were insured [1]. Climate change effects extend beyond economics to human health and well-being. Disaster databases show that power outages and heat waves, resulted in over 62,000 heat-related deaths in Europe in 2022 alone, and that the most vulnerable groups are disproportionally affected [2] particularly in southern Europe where heat-related deaths are increasing steadily [3]. Buildings, responsible for 40 % of energy consumption, 36 % of greenhouse gas emissions, and 35 % of waste [4], need urgent decarbonization to mitigate these climate impacts. However, even with net-zero goals, existing atmospheric carbon will continue to impact communities for decades [5], and these impacts are worsened by natural disasters such as earthquakes, which caused over 200,000 deaths and €250 billion in damage in the 20th century [6]. Integrating disaster-resilience-thinking into research, practice and policy is therefore crucial to minimize future losses.

As a result, there has been a rise in risk and resilience assessments, methods and digital tools for assets, infrastructure and human communities (e.g., Refs. [7–11]). More specific resilience considerations for buildings have been introduced in the REDi design guidelines [12–14], establishing resilience objectives and a roadmap to enhance building performance before, during and after disruptive events. These approaches are helpful, but they are primarily qualitative and therefore lack the incisiveness of quantitative methods. Resilience is defined by the ability of a building to "bounce back" to a new equilibrium within a recovery time after absorbing the impact of an external natural or man-made event, and is traditionally measured by metrics based on the so-called 4R's of resilience [15]: (1) *Robustness* (R1) - the ability of a building to endure without loss of functionality; (2) *Redundancy* (R2) - the ability of a building to provide alternative options under stress; (3) *Resourcefulness* (R3) - the extent to which resources can be mobilized during emergencies; (4) *Rapidity* (R4) - the rate of recovery. The first two metrics influence the so-called "Response phase", while the last two pertain to the "Recovery phase" of the resilient behaviour of a system (Fig. 1a).

In events such as earthquakes, windstorms and floods, resilience metrics typically focus on physical vulnerability. Building robustness is measured by damage quantification and fragility curves, which provide the system's probability of achieving or exceeding predefined performance levels for specific hazard intensities (e.g., Refs. [16,17]). Fragility curves, which are extensively used in earthquake engineering to quantify structural vulnerability at component to building level, have also been adapted for other hazards such as flood and wind (e.g., Refs. [18,19]). Redundancy refers to the presence of "backup" components, e.g. multiple HVAC units and/or supplemental electrical generators and water storage supply in hospitals for continuity of operation, and their additional capacity to meet demands during failures; redundancy can enhance the robustness by reducing the severity of failure. Recovery capacity, which integrates both resourcefulness and rapidity, is instead measured through restoration functions. These functions assess progress towards a recovery state using factors such as financing availability, permitting processes, repair logistics and restoration of utilities [12–14]. Resilience is typically assessed by assuming a time-invariant system functionality prior to the occurrence of an extreme event and after the completion of the restoration process. However, environmental aggressiveness can cause progressive damage that gradually reduces system functionality over time, thus altering the impact of extreme events of the same magnitude. To address this, several studies have examined the progressive degradation of system performance and its implications for resilience quantification, particularly within the context of life-cycle resilience analysis [e.g., 20,21].

For heat hazards, resilience metrics account for building thermal behaviour, and recent literature [22–24] highlights the growing need for multi-criteria frameworks to assess and enhance resilience. Prolonged exposure to heat stresses can lead to changes or fluctuations in a building's functionality. Resilience is assessed by defining thresholds of air temperature or combined indices (e.g., operative temperature or standard effective temperatures), beyond which thermal exposure becomes uncomfortable or poses heat-related health risks. Building cooling measures ensure resistance and robustness against these conditions. Recovery is usually quantified as the time required to return to acceptable thermal conditions and ensure occupant safety. Cooling measures can also provide redundancy when multiple units are designed to maintain thermal comfort even if one fails, as seen in hospitals, or when integrated with passive cooling strategies as natural ventilation. Research studies on heat resilience are emerging (e.g., Refs. [25–27]),

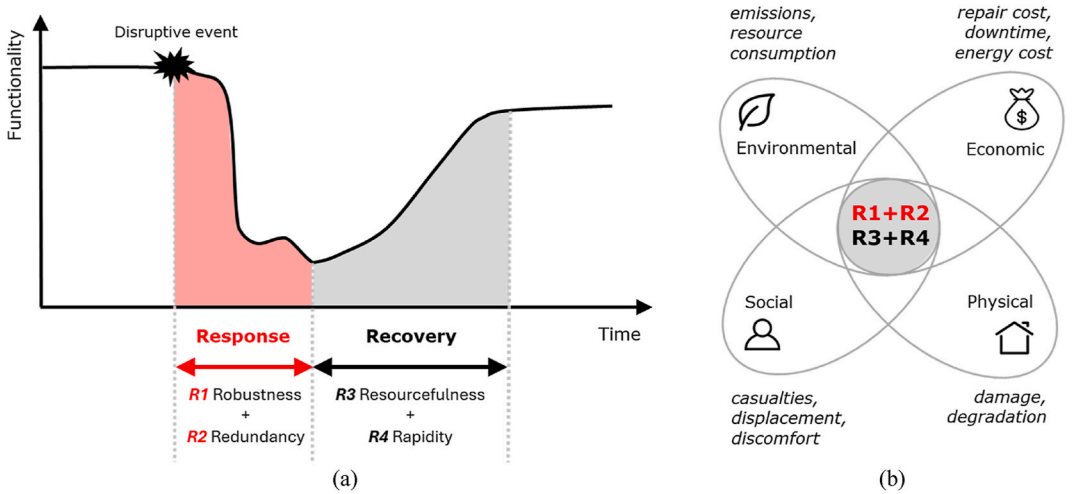

Fig. 1. Phases (a) and domains (b) of Resilience.

but this field is still in its infancy and requires the development of robust frameworks to define specific threshold levels, boundary conditions related to human behavior and power availability, and appropriate hazard models. Further research on human illness and mortality is critical since the exposure of individuals depends on their location and can be influenced by urban heat islands, microclimates and differences between indoor and outdoor temperatures.

Despite these advancements across various engineering disciplines, traditional and current approaches often address only single

Table 1
Resilience indicators.

Hazard	Phase	Domain	Indicator	Description	Reference	Index	Normalization
Heat	Response	Social	$CDH_{SET\,min-crit}$	Cumulative degree hours between SET minimal and critical [°h]	[23,53]	I_{H-Res1}	$\frac{CDH_{SET\,min-crit}}{SET_{reference} \cdot Ref.\,period}$
			$CDH_{SET\,crit}$	Cumulative degree hours after SET critical [°h]	[23,53]	I_{H-Res2}	$\frac{CDH_{SET\,crit}}{SET_{reference} \cdot Ref.\,period}$
			ND_H	Number of deaths	[43]	I_{H-Res3}	$\frac{ND_H}{Building\ occupants}$
		Environmental Economic	E_{Res}	Cooling energy consumption [kWh/m^2]	[23]	I_{H-Res4}	$\frac{E_{Res}}{E_{reference}}$
	Recovery	Social	$T_{SET\,crit}$	Time to return to SET critical [h]	[22]	I_{H-Rec1}	$\frac{T_{SET\,crit}}{Ref.\,period}$
		Environmental Economic	E_{Rec}	Cooling energy consumption [kWh/m^2]	[23]	I_{H-Rec2}	$\frac{E_{Rec}}{E_{reference}}$
Earthquake	Response	Physical	$MAFC$	Mean Annual Frequency of Collapse	[46]	I_{E-Res1}	$\frac{MAFC_{damaged}}{MAFC_{undamaged}}$
			$\%NBS$	% New Building Standard	[44,45]		$\frac{Capacity_{As-Build}}{Capacity_{NewBuild}}$
			$MAFE_E$	Mean Annual Frequency of Exceedance of a Limit/Damage State [1/years]	[46]		$\frac{MAFE_E}{MAFE_{EDS\ threshold}}$
			RDR	Residual Drift Ratio	[16]	I_{E-Res2}	$\frac{RDR}{RDR_{threshold}}$
		Social	ND_E	Number of deaths	[16]	I_{E-Res3}	$\frac{ND_E}{Building\ occupants}$
		Economic	RC_E	Repair Cost [cost/m^2]	[16]	I_{E-Res4}	$\frac{RC_E}{Replacement\ cost}$
	Recovery	Social	D_E	Number of displaced people	[54]	I_{E-Rec1}	$\frac{D_E}{Building\ occupants}$
		Economic	DT_E	Downtime [months]	[12]	I_{E-Rec2}	$\frac{DT_E}{Replacement\ time}$
		Environmental	CE_E	Carbon emissions [kg $CO2_e$/m^2]	[16]	I_{E-Rec3}	$\frac{CE_E}{Replac.\ carbon\ footprint}$
Wind	Response	Physical	$MAFE_W$	Mean Annual Frequency of Exceedance of a Limit/Damage State [1/years]	[47]	I_{W-Res1}	$\frac{MAFE_W}{MAFE_{WDS\ threshold}}$
		Social	ND_W	Number of deaths	[16]	I_{W-Res2}	$\frac{ND_W}{Building\ occupants}$
		Economic	RC_W	Repair Cost [cost/m^2]	[16]	I_{W-Res3}	$\frac{RC_W}{Replacement\ cost}$
	Recovery	Social	NAP_W	Number of affected people	[50]	I_{W-Rec1}	$\frac{NAP_W}{Building\ occupants}$
		Economic	DT_W	Downtime [months]	[14]	I_{W-Rec2}	$\frac{DT_W}{Replacement\ time}$
		Environmental	CE_W	Carbon emissions [kg $CO2_e$/m^2]	[16]	I_{W-Rec3}	$\frac{CE_W}{Replac.\ carbon\ footprint}$
Flood	Response	Physical	RF	Resistance of facades to floods	[49]	I_{F-Res1}	$\frac{RF}{RF_{reference}}$
			BFP	Flooded building perimeter	–	I_{F-Res2}	$\frac{BFP}{Tot.\ perimeter}$
			ABF	Area of flooded building facades	–		$\frac{ABF}{Tot.\ envelope\ area}$
		Social	ND_F	Number of deaths	–	I_{F-Res3}	$\frac{ND_F}{Building\ occupants}$
		Economic	RC_F	Repair Cost [cost/m^2]	[55]	I_{F-Res4}	$\frac{RC_F}{Replacement\ cost}$
		Environmental	WD	Water depth	[56]	I_{F-Res5}	$\frac{WD}{WD_{Reference}}$
			FV	Flow velocity	[56]	I_{F-Res6}	$\frac{FV}{FV_{Reference}}$
	Recovery	Social	NAP_F	Number of affected people	[55]	I_{F-Rec1}	$\frac{NAP_F}{Building\ occupants}$
		Economic	DT_F	Downtime [months]	[13]	I_{F-Rec3}	$\frac{DT_F}{Replacement\ time}$
		Environmental	CE_F	Carbon emissions [kg $CO2_e$/m^2]	[16]	I_{F-Rec4}	$\frac{CE_F}{Replac.\ carbon\ footprint}$

hazards, failing to support decision-making for integrated resilience strategies. In recent years, multi-hazard approaches have emerged to enable more comprehensive resilience assessments. These methods employ either simplified multi-criteria decision-support procedures (e.g., Refs. [28–31,60]) or more robust probabilistic-based methodologies that account for hazard interactions and/or physical vulnerability interactions for specific scenarios or across the building's lifecycle (e.g., Refs. [32–34]). However, most of these studies focus on dual-hazard interactions, such as seismic-flood or seismic-wind, while broader hazards combinations are typically unexplored. In particular, heat-related vulnerabilities, which increasingly affect communities and the environment through overheating and rising energy demand, are not integrated into these frameworks. Indicator-based approaches have also emerged, especially in seismic resilience assessment (e.g., Refs. [30,35,36]), to capture the effects of different dimensions such as damage, repair cost and downtime. Nonetheless, the full spectrum of potential consequences is rarely considered, often omitting a comprehensive evaluation of the four key resilience domains: physical, social, economic and environmental [37]. Both single-hazard and multi-hazard assessments would benefit from the adoption of holistic metrics that integrate multi-criteria indicators spanning all these domains (Fig. 1b).

Embedding resilience indicators into early-stage decision-making can lead to cost-effective, sustainable, safe, comfortable and resilient building designs and retrofits, as initial decisions affect up to 80 % of the final choices [38], making this phase crucial to enhance building sustainability and resilience. This study provides a practical decision-support framework for early-stage multi-hazard multi-domain resilience design and evaluation of individual buildings. Specifically, the study: (i) defines a comprehensive set of resilience indicators - either derived from existing literature or newly proposed - addressing structural safety, energy efficiency, carbon emissions, occupant well-being and cost; (ii) establishes holistic Resilience Readiness indices to assess resilience against single or multi-hazard risk scenarios, incorporating post-event response and recovery phases; and (iii) develops rating systems to support decision-makers in conducting impact assessments and categorizing individual buildings according to their Resilience Readiness Level. A key novelty of the study lies in the systematic organization and normalization of heterogeneous indicators, enabling consistent comparison across different hazard types and resilience domains at the building scale. This step is critical for achieving an integrated and comparable resilience assessment. Furthermore, contributions (ii) and (iii) represent an innovative application of the hybrid AHP-TOPSIS [39] decision-making method to the context of building-level resilience - an approach that, to date, remains underexplored in the literature for operationalizing multi-domain and multi-hazard resilience assessments at the scale of individual buildings. The proposed framework moves beyond treating each hazard in isolation and instead supports the evaluation of combined impacts within a unified scenario.

The paper is organized as follows: Section 2 describes the research method, which includes the definition of multi-domain resilience indicators, their quantification and integration into holistic resilience scores; Section 3 applies the proposed method to urban blocks, characterized by different building archetypes and local hazards (The Netherlands, Italy); Section 4 discusses potential applications for building resilience assessment and design; Section 5 presents the main conclusions of the work.

2. Research method

This research was developed as part of the Horizon Europe MULTICARE project [40], aiming to advance resilience design, assessment and management of buildings through a multi-hazard perspective across various scales (component, building, urban). Central to the project development is the definition of multi-criteria indicators to measure building resilience against heatwaves, earthquakes, windstorms and floods. These indicators are crucial for integrating resilience considerations into the complex multi-disciplinary design process of buildings, enabling to assess their resilience capacity and systematically compare alternative holistic mitigation and adaptation strategies.

2.1. Multi-domain resilience indicators

Measurable resilience indicators were defined from literature references, current standards and practice, with a specific focus on quantitative parameters derived from building performance simulations and risk assessment. These indicators, summarized in Table 1,

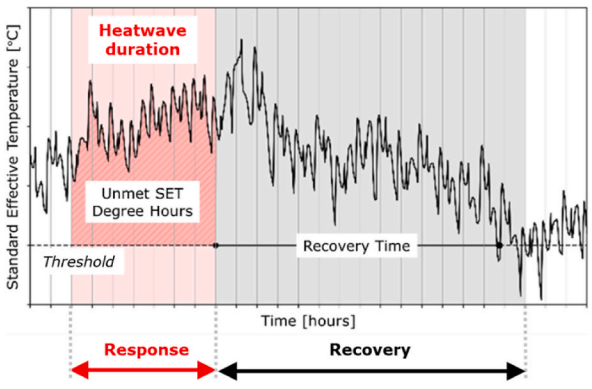

Fig. 2. Functionality-time (resilience) curve for heatwave scenarios based on the $CDH_{SET\,crit}$ definition.

describe a building's overall capacity to respond to and recover from different extreme events.

Heat resilience is associated with the heat vulnerability of buildings, specifically how heatwaves impact both the buildings and their occupants. The thermal response of a building is affected by construction materials and quality, cooling measures (passive or active) and occupant behaviour. Although the physical (structural) domain is not particularly relevant for this hazard, since the structural integrity of building components is not significantly compromised by heat, the impact on the other domains is notable. The human response to extreme heat events can be assessed by means of the Standard Effective Temperature (SET), defined as the dry-bulb temperature in a hypothetical environment with 50 % relative humidity [41]. Relevant heat resilience indicators include Cumulative Degree Hours (CDH) between SET minimal (lowest effective temperature at which thermal comfort is still maintained) and SET critical (effective temperature at which thermal conditions become hazardous or uncomfortably extreme), identified below as $CDH_{SET\,min-crit}$, as well as the CDH after SET critical ($CDH_{SET\,crit}$) and the cumulative time from SET critical to SET minimal ($T_{SET\,crit}$). These indicators capture both the intensity of thermal conditions and the duration of exposure. This is illustrated in Fig. 2 through the $CDH_{SET\,crit}$, where the critical SET threshold can be defined based on relevant guidelines, expert judgment or established frameworks [42]. Heatwave duration refers to the consecutive period during which temperature exceeds a defined threshold for a minimum number of days, as determined by local institutions or regulatory guidelines (e.g., the World Meteorological Organization defines a heatwave as "a period of more than five consecutive days during which the daily maximum temperature exceeds the average maximum temperature by 5 °C, with the reference period being 1961–1990").

By analysing temporal variations in heat-mortality associations derived from recorded data (e.g., Refs. [3,43]), the impact of extreme temperatures on mortality risk can also be assessed. Beyond social impacts, it is important to quantify the monetary and environmental losses associated with operating cooling systems to maintain acceptable indoor thermal conditions during heatwaves, as reflected in their operational costs and the carbon emissions from energy consumption.

For events causing structural damage, the physical impact on buildings is quantified to define their response capacity. In the context of earthquakes, this impact can be assessed through indices that describe the building's damage or safety level and its residual capacity, particularly important in case of aftershocks. In accordance with code-compliant procedures, the safety level can be evaluated by comparing the building's Capacity to the Demand - minimum code requirements - of a new structure. This Safety Index, represented by the %NBS (percentage of New Building Standard) in the NZSEE2017 Assessment Guidelines [44] or the IS-V (Life Safety Index) in the Italian 2017 Seismic Classification Assessment Guidelines, DM 65 [45], is typically used by engineers, insurance companies and government agencies to assess a building's seismic risk and identify the need for retrofitting. An alternative indicator to describe the safety level is the Mean Annual Frequency of Exceedance (MAFE), which represents the annual probability of exceeding a certain limit state (structural safety and/or building serviceability) [46]. To quantify the residual capacity of a damaged structure, which is essential for decisions on repair, retrofit or demolition, the MAFE before (undamaged) and after (damaged) an earthquake can be used to determine the ratio of the Mean Annual Frequency of Collapse (MAFC). An alternative and complementary indicator, based on typical Engineering Demand Parameters (EDP), is the Residual Drift Ratio (RDR), measuring the permanent residual deformation of a building after an earthquake and expressed as the ratio of overall seismic displacement to the height of a floor or the entire building [14]. For wind loading, physical resilience can be assessed using similar indicators. The MAFE of a limit or damage state can be used to measure structural safety, building serviceability and user comfort [47], and quantified using the SAC-FEMA probabilistic approach adapted for wind loading [48]. Focusing on flood events, damage assessment depends on both the physical characteristics of buildings and the mechanical impact of water, described by water depth and flow velocity. Water depth measures the height of the water layer from ground level, while flow velocity indicates the potential of the flood to cause erosion, increase structural damage and transport sediments and debris. Quantifying these indicators enables stakeholders to implement effective water management measures, such as levees, embankments, lateral structures and ponds. To define physical damage, the resistance of building envelopes to floods is a key indicator, reflecting a building's impermeability and defined based on the type of materials used for the windows and walls, and the quality of the joints [49]. Additional indicators include the flooded building perimeter, which measures the extent of flooding around it, and the surface area of building envelope affected by flooding, providing insight into water impact on the building's exterior.

The impact of earthquakes, wind and floods extends beyond structural damage to affect other resilience domains. These hazards significantly impact the safety and well-being of building occupants. Earthquakes can cause partial or total collapse of structural (skeleton) and non-structural (architectural components, contents, services) elements, leading to injury or loss of life in the aftermath of the event, and causing people displacement during the recovery phase. Wind can damage building envelopes and roofs, resulting in water ingress and affecting people in various ways, ranging from serviceability loss to injuries and/or displaced people due to the unserviceability of houses [50]. Floods can disrupt communities by inundating buildings and causing similar displacements. In each case, it is essential to estimate casualties and the number of displaced individuals as resilience indicators for effective response planning and emergency management. The damage caused by these events also leads to economic losses. Assessing the direct financial impact, i.e. repair or replacement costs, is crucial for prioritizing resources and planning interventions during the response phase. The indirect economic loss, on the other hand, serves as a resilience indicator to define the post-disaster recovery of the building, and it entails delays in scheduling inspections, mobilizing workers and materials, securing financing for repairs and the repairs themselves [12–14]. This downtime disrupts daily activities, resulting in lost income and relocation expenses for affected occupants. Beyond economic indicators, the disposal of debris and the repair or replacement of building components contribute to carbon emissions and environmental degradation. Since resilience is inherently a key aspect of sustainability, it is essential to quantify the carbon footprint associated with extreme events, considering embodied carbon, energy use, material resource use and waste generation.

All the aforementioned indicators can be computed for a specific event to estimate their probable value (intensity or scenario based assessment). In this case, losses are quantified as the probability of exceeding a certain threshold across a range of outcomes, from which a Probable Maximum Loss (PML) can be derived. Time-based assessments can also be implemented to quantify the Expected

Annual Loss (EAL), which describes the probable performance of a building over a specified period, considering all potential events and their probabilities. EAL is a key metric for cost-benefit analyses and for determining appropriate insurance premiums. The choice of the assessment type (intensity-based, scenario-based or time-based) and the corresponding resilience indicators depends on the stakeholder and specific application. For example, an insurance company would prioritize quantifying the probability of incurring a specific payout for an event of a given intensity to ensure financial solvency. Moreover, as discussed in Section 2.5, the resilience indicators support the integration of regional variations into the assessment, thereby enabling a more context-sensitive evaluation of how different hazards impact building performance [e.g., 51,52].

2.2. Indicator normalization

The resilience indicators identified for each hazard have different units, therefore, normalization is performed (Table 1) to facilitate effective comparison and aggregation into a final multi-criteria index (Sections 2.3, 2.4). This process prevents any single indicator from dominating due to scale differences and enables meaningful weighting by placing the indicators on a common scale (if no weights are applied, all indicators are implicitly treated as equally important). As discussed below, normalization is carried out by dividing each resilience indicator by a relevant reference or threshold value representing its worst-case scenario. Consequently, lower values reflect greater system resilience in relation to that specific aspect.

Heat resilience indicators are derived from building energy performance simulations conducted over an entire year (time-based) or specifically for the duration of a heatwave (intensity or scenario based), with the selected time period used to normalize social indicators accordingly as outlined in Table 1 ($I_{H-Res1}, I_{H-Res2}, I_{H-Rec1}$). Reference values for SET (I_{H-Res1}, I_{H-Res2}) are based on human comfort thresholds, and can be derived from existing guidelines such as ASHRAE Standard [41], while the number of deaths (I_{H-Res3}) can be normalized by the number of building occupants. When evaluating heat-related economic and environmental indicators (I_{H-Res4}, I_{H-Rec2}), threshold values can be established either by scientific literature, input from decision-makers or public health recommendations, which are typically defined at the national level (as shown in Section 3).

For the other hazards, some indicators are inherently normalized (I_{E-Res1} - *MAFC* or *%NBS*), while others can be normalized based on building properties (I_{F-Res2}). Thresholds for other physical indicators can be derived from existing standards or guidelines (e.g., FEMA P-58 [16] for I_{E-Res2}, FEMA 2008 [49] for I_{F-Res1}), literature (e.g., Franchin & Noto [57] for $I_{E-Res1} - MAFE_E$), or current practice. For flood impacts, thresholds for water depth or flow velocity (I_{F-Res4}, I_{F-Res5}) can be based on levels where significant or total losses occur, if exceeded. For example, in areas prone to severe flooding or extreme vulnerability, the 0.1 % return period is typically used to guide long-term planning and mitigation efforts. Social indicators, including both deaths ($I_{E-Res3}, I_{W-Res3}, I_{F-Res3}$) in the response phase and the displaced or overall affected people in the recovery ($I_{E-Rec1}, I_{W-Rec1}, I_{F-Rec1}$), can be normalized by the number of building occupants, while economic (repair cost - I_{E-Rec2}, I_{W-Rec2}, I_{F-Rec2}, and downtime - I_{E-Rec3}, I_{W-Rec3}, I_{F-Rec3}) and environmental indicators (I_{E-Rec4}, I_{W-Rec4}, I_{F-Rec4}) are normalized relative to the associated replacement value of the building.

It is observed, however, that some adaptations may be needed in the normalization process, as certain indicators may yield values close to 0 by definition (e.g., EAL). To ensure proper comparison with other indicators, it is necessary to redistribute these values more evenly along the scale. As discussed in Section 3, a logistic distribution can be used to address this issue as: (i) it ensures the function's range aligns with the decision-making problem, (ii) the distribution is more sensitive around values that mark a shift from desirable to undesirable outcomes, while grouping extreme values together, reducing the impact of small changes in those areas.

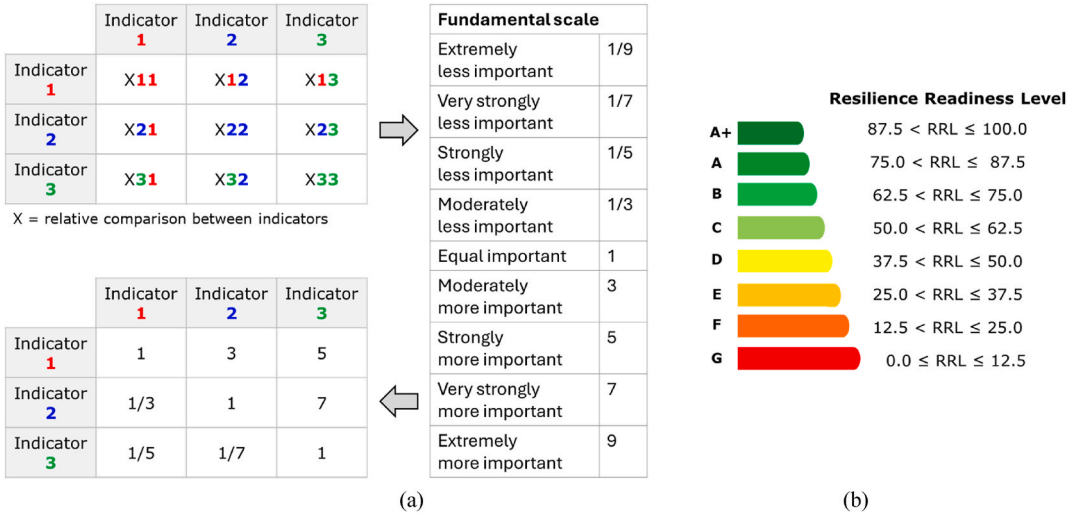

Fig. 3. (a) Schematic representation of the pairwise comparison process. (b) Labelling system for Resilience Readiness Level (*RRL*).

2.3. Single-hazard resilience score

The normalized indicators are combined into hazard-specific Resilience Readiness (*RR*) indices which characterise the holistic resilience of a building, reflecting its capacity to respond and recover from an extreme event. Following an approach similar to Bertilsson et al. [28], the resilience phases are treated as sub-indices (RR_{Res} - Eq. (1), RR_{Rec}- Eq. (2)) and are calculated using a geometric aggregation of the normalized indicators (Section 2.2) subtracted from unity – where values closer to 1 indicate high resilience. While linear aggregation is also possible, the geometric method was selected in this study to reflect the compounding effects of weaknesses across different resilience indicators.

$$RR_{Res} = 1 - \prod_{i=1}^{n} I_{Res_i}^{w_{Resi}} \tag{1}$$

$$RR_{Rec} = 1 - \prod_{i=1}^{m} I_{Rec_i}^{w_{Reci}} \tag{2}$$

Different and specific weights can be assigned to reflect the relative importance of each resilience indicator within the response and recovery phase (w_{Resi}, w_{Reci}). When more than three normalized indicators are considered in the calculation of RR_{Res} and RR_{Rec}, the Analytic Hierarchy Process (AHP) [58] can be used to determine these weights through pairwise comparisons. The relative comparison (x_{ij}) between two indicators (i and j) is defined using a scale ranging from 1 (equal importance) to 9 (extremely more important) (Fig. 3a). The overall resilience score (*RR*) is then calculated using a linear aggregation of the two phases, applying phase-specific weights (w_{Res}, w_{Rec}) to account for their relative priority (Eq. (3)).

$$RR = RR_{Res} \cdot w_{Res} + RR_{Rec} \cdot w_{Rec} \tag{3}$$

To classify the *RR* index for a specific hazard, a universal rating scale can be defined to determine the Resilience Readiness Level (*RRL*) of a building. Based on proposed resilience classification schemes [59] and existing labelling systems for energy efficiency and seismic risk [60], this scale is divided into eight classes, translating numeric scores (*RR*, ranging from 0 to 1) into resilience grades (*RRL*, ranging from 0 % to 100 %, with 100 % indicating no impact on the building from the extreme event). The resilience classes range from F to A+ (where A+ represents higher resilience and G indicates low resilience); this approach makes resilience levels more understandable and intuitive to stakeholders (Fig. 3b).

2.4. Multi-hazard resilience score

When considering a multi-hazard scenario, the RR_{Res} andRR_{Rec} values for different hazards can be combined to derive a comprehensive multi-hazard resilience score for buildings, thereby allowing direct comparisons of the resilience levels of as-built, newly designed or retrofitted structures under various hazard conditions. This score can be derived by implementing two compensatory decision-support methods in a hybrid mode: (i) the AHP [58], to determine weighting for the $RR_{Res/Rec}$ values (performance criteria) and (ii) the Technique for Order of Preference by Similarity to Ideal Solution (TOPSIS) [61], to rank different buildings (Fig. 4). TOPSIS provides a measure of how far each alternative is from the ideal solution (S_i^+), representing the best possible performance values for each criterion, and from the negative ideal solution (S_i^-), being the worst possible performance values for each criterion. The relative closeness (C_i^*) to the ideal solution can thus be quantified (Eq. (4)), representing the final resilience score (where the highest relative closeness indicates higher resilience).

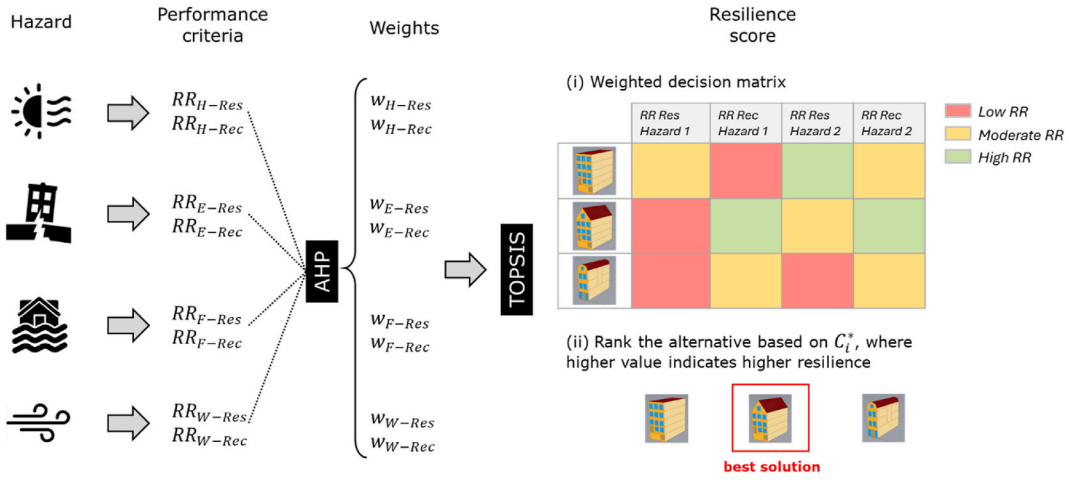

Fig. 4. Multi-hazard resilience scoring using a hybrid AHP-TOPSIS approach.

$$C_i^* = \frac{S_i^-}{S_i^+ + S_i^-} \tag{4}$$

In this way, AHP ensures consistent and reliable portrayal of the relative importance of each criterion, while TOPSIS provides computational efficiency, requiring only simple arithmetic operations, and its ease of understanding through the concept of proximity to an ideal solution. Combining AHP for weighting and TOPSIS for ranking leverages the strengths of both methods for comprehensive multi-criteria resilience assessment of buildings and their components [39].

2.5. Weight definition

In the proposed framework, two levels of weighting are considered: (i) indicator-level weights, assigned to individual indicators within each phase to capture their specific contribution to overall phase-level resilience; (ii) phase-level weights, used in the aggregation of the response and recovery phases to obtain the overall resilience score. Variations in these weight assignments can significantly affect the calculated resilience scores and, in turn, influence decision-making - particularly for buildings that are highly sensitive to specific hazard types. Therefore, careful and context-sensitive weight definition is essential to ensure that decisions align with the specific characteristics and priorities of the problem at hand.

As discussed above, when more than three indicators and/or hazards are considered in the assessment, a pairwise comparison matrix can be constructed to obtain weight coefficients. Each element of the matrix represents the judgment of the decision-maker on the importance of one element (indicator/phases) over another using a predefined scale (typically the Saaty scale, ranging from 1 to 9 - Fig. 3a). These judgments are then processed to compute normalized weights reflecting the relative priority of each element [58]. Since the matrix reflects the priorities of decision-makers, these should be informed by the local hazard context, building function or typology and the specific objective of the analysis - e.g., whether it involves resilience-informed design or planning for intervention. Stakeholders can tailor the definition of weights based on the dominant hazard types in their region, guided by an initial screening of local hazard exposure. For example, in regions where seismic risk is predominant, higher weights may be assigned to indicators related to structural integrity and performance. In contrast, flood-prone areas may prioritize indicators associated with water ingress resistance or site elevation. Similarly, building use plays a crucial role: (i) for a hospital, indicators related to operational continuity and human safety might be prioritized, while (ii) in residential buildings, emphasis may be placed on affordability and repair time. In a retrofitting scenario, decision-makers may prioritize solutions that are cost-effective, quick to implement and involve minimal health and safety risks. In sustainability-driven projects, carbon emissions may carry more weight, especially if emissions reduction aligns with broader policy goals. These context-specific considerations should guide the pairwise comparisons in the matrix to ensure that the resulting weights support actionable resilience evaluations. Drawing on relevant policies and stakeholder workshops, future work could focus on developing weighting matrices for specific hazard scenarios and building typologies, in order to promote consistent and context-appropriate weight definition across diverse applications.

Given the reliance on expert judgment, the resulting weight coefficients are subject to epistemic uncertainty. This stems from the subjective nature of the pairwise comparisons. To address this, a consistency ratio (CR, Eq. (5)) is calculated to assess the internal logic of the comparison matrix. A $CR \leq 10$ % is generally accepted as an indicator of adequate consistency.

$$CR = \frac{CI}{RI} \text{ where } CI = \frac{\lambda_{max} - n}{n - 1} \tag{5}$$

Where, λ_{max} is the principal eigenvalue of the matrix, n is the order (i.e., number of criteria), and RI is the random index, which depends on n. This process ensures that the derived weights are not only tailored to the specific problem but also logically consistent, improving the robustness and interpretability of the resilience assessment.

The framework is therefore designed to accommodate context-specific weighting schemes to ensure meaningful results in diverse multi-hazard scenarios. While the AHP provides a structured method for deriving weights based on expert judgment and stakeholder input, other objective weighting methods can also be employed to minimize bias. For example, the CRITIC method (CRiteria Importance Through Intercriteria Correlation) evaluates weights by considering both the contrast intensity of criteria and the degree of conflict or correlation among them [62]. Nonetheless, although objectively derived weights are grounded in statistical properties, they may not fully capture contextual priorities; therefore, integrating subjective and objective approaches through hybrid methods could be used for balanced decision support.

2.6. Hazard interdependencies and correlations between resilience indicators

Resilience indicators may exhibit degrees of correlation. For instance, repair costs and CO_2 emissions are somewhat correlated with the *%NBS* and the *MAFE*. These system-specific correlations are largely influenced by the design configuration. Accordingly, the implementation of efficient design strategies (e.g., structural material optimization) or the adoption of new technologies (e.g., sustainable construction materials and methods) can alter these relationships, particularly among indicators belonging to different resilience domains (e.g., environmental and social, as in the case of CO_2 emissions vs. *%NBS* or *MAFE*). In contrast, environmental correlations are more complex and inherently harder to manage, yet they can significantly influence system resilience. One of the most critical forms of environmental correlation arises from interactions between multiple hazards. Neglecting such multi-hazard (MH) interactions can lead to an underestimation of potential damages and losses. In MH scenarios, hazards may occur independently, simultaneously (i.e., in a correlated manner) or sequentially in cascading chains [63]. These interactions can manifest at various levels.

- *Action level:* for example, when flash flooding occurs during a severe windstorm with heavy rain, a building envelope may be subjected simultaneously to hydraulic and wind actions.
- *Structural vulnerability level:* an earthquake may damage a structure, increasing its vulnerability to a subsequent hazard, such as a tsunami triggered by the seismic event.
- *Design strategy level:* a design decision targeting one hazard (e.g., selecting a façade for heatwave mitigation) may influence design requirements related to another (e.g., limiting inter-story drift under wind loads).

All the aforementioned MH cases can be incorporated into the proposed framework as distinct scenarios. Although rare over a building's life cycle (i.e., low probability of occurrence), they can be evaluated using the same set of indicators employed for single-hazard assessments. For instance, an earthquake-triggered tsunami scenario would lead to elevated flood-related indicators, which could be quantified through dedicated simulations and considered as additional contributions relative to flood-only conditions. The proposed framework can accommodate hazard interactions by properly evaluating how these interactions affect indicators and, in turn, influence resilience metrics. This is achieved through a structured two-step process.

- *Preliminary Hazard Interaction Screening.* As a first step, a preliminary screening of possible interactions is conducted between hazards (pairwise), based primarily on the exposure of the structure. For instance, a tall building located in a flood-prone area is a candidate for compound wind-flood effects. This screening helps identify plausible multi-hazard scenarios that warrant specific attention.
- *Identification and Adjustment of Affected Indicators.* When potential interactions are identified, resilience indicators sensitive to such interactions are determined. These interactions manifest differently depending on the phase (Response or Recovery) and indicator domain. In the Response phase, certain indicators might exhibit complete overlap, such as "Number of deaths" under the social domain. In such cases, double-counting can be avoided by assigning impacts to the specific hazard responsible. For example, if a fatality is caused by wind during a compound wind-flood event, it is recorded solely under the wind-related indicator. In the Recovery phase, interactions are often amplified due to resource constraints and cascading effects. For example, downtime resulting from wind damage might be significantly prolonged if floodwaters delay access or overload response capacities. Concurrent hazards can stress the available recovery resources, leading to extended delays even in cases where individual hazards might not have had such impact in isolation. Additionally, long recovery times may trigger threshold effects, where after a certain delay, repairs become economically or socially unfeasible. The framework is capable of capturing such time-sensitive nonlinearities through time-based adjustments in the Recovery indicators.

The current framework is therefore capable of accounting for compound effects through scenario-based adjustments and indicator disaggregation. Future extensions will build upon this foundation by formalizing coupling mechanisms within composite indicators to more explicitly represent the combined impacts of multiple hazards. To further enhance the understanding of interdependencies among resilience indicators, data-driven techniques such as Artificial Neural Networks (ANNs) [64] could be employed. These models are well-suited to capturing nonlinear relationships and may complement traditional decision-making approaches by deriving data-informed weights.

3. Application to real-world case studies

The proposed approach was applied to quantify the resilience of buildings under both (i) a single-hazard scenario (heatwave) in Amsterdam, The Netherlands, and (ii) a multi-hazard scenario (earthquake, heatwave, flood, wind) in Acerra, province of Naples, Italy. Key resilience indicators were defined to support decision-making for the two scenarios, which involved establishing an initial baseline characterization of the as-built structures. This aligns with the current stage of the MULTICARE project [40], where the selected urban blocks serve as virtual demonstration sites for testing and validating the methods and digital tools developed. The project leverages diverse climates and architectural styles to provide a range of real-world conditions and urban environments for evaluation, bringing

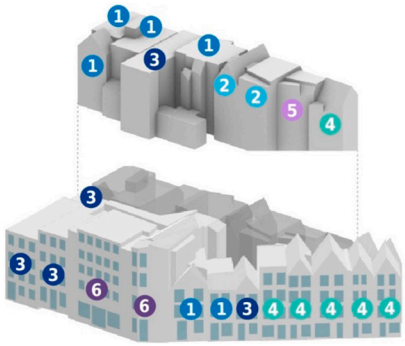

	No. floors	Compactness ratio	Ground floor area [m^2]	Total floor area [m^2]
1	5	0.30	60	300
2	5	0.30	60	300
3	5	0.45	60	300
4	4	0.45	50	200
5	4	0.45	50	200
6	4	0.45	130	310

Fig. 5. Exploded isometric perspective of the urban block analyzed in Amsterdam, with index numbers indicating the building archetype.

together multidisciplinary experts from across Europe.

3.1. The Amsterdam case study

In a 2023 survey conducted by the Centre of Expertise City NetZero [65], 90 % of respondents indicated that they experienced heat stress in their homes during heatwaves in the Amsterdam centre district. They described the temperatures in their bedrooms and living rooms as "too hot" or "much too hot". By 2050, the number of overheated buildings in Amsterdam is expected to rise even under a low-emission scenario (SSP1-2.6), which predicts a 1.7 °C temperature rise [66]. Heatwaves are therefore critical for the city and this hazard was considered for the resilience score calculation of an existing mixed-use block in the inner city. Specifically, six building archetypes with diverse properties were identified within the urban block (Fig. 5, where the compactness ratio represents the ratio of all exposed envelope surfaces to the total building volume), characterized by residential or mixed use with commercial spaces on the first floor, with or without cooling systems (Table 2).

Daily climate observations from Amsterdam Schiphol Airport station for the period 1951–2023 were obtained from the NOAA dataset [67]. The heatwave definition CTX90pct [68], which identifies a heatwave as a period when the maximum daily temperature exceeds the 90th percentile for at least three consecutive days, was used to select the historical heatwave year for simulation. Using the CTX90pct criterion, the event on July 23–27 2019 was identified as the heatwave with the highest maximum daily temperature (36.4 °C). Fig. 6a shows the hourly dry bulb temperature during the 2019 heatwave period compared to the Typical Meteorological Year (TMY). The 2019 heatwave saw temperature differences up to 15 °C above the typical year for the five days it took place, with temperatures returning to typical levels afterward.

Building dynamic energy simulations were conducted to derive heat resilience indicators and assess the buildings *RR* value under the selected heatwave scenario. The energy simulations were performed in Rhinoceros 3D using the parametric interface of Grasshopper, a graphical algorithm editor that enables energy simulations with EnergyPlus [69]. Building layouts were defined using the data from Table 2 and divided into energy zones according to occupancy and thermal properties. Data from an *in-situ* energy motoring study was used to calibrate these models [70]. For this specific application, four indicators were chosen from Table 1: $CDH_{SET\,crit}$ and E_{Res} to describe the building's response, and $T_{SET\,crit}$ and E_{Rec} to define the recovery phase. The simulation was run twice for each archetype: once with natural ventilation and once with a cooling system operating from 7 a.m. to 7 p.m., with a setpoint temperature of 25 °C. The analysis did not account for the impact of the urban context (heat island effect). An ideal loads air system, auto sized using the TMY weather data, was assumed.

SET indicators were computed from the natural ventilation scenario, while energy consumption indicators came from the cooling system scenario (Fig. 6b). In calculating RR_{Res}, a 5-day heatwave served as the reference period for the indicators normalization. $CDH_{SET\,crit}$ measured the cumulative degree hours above SET 30 °C [71] during the heatwave, normalized by the degree hours of exceeding SET 30 °C by at least 5 °C (assumed $SET_{reference}$) over the same period. E_{Res} measured cooling energy consumption during the heatwave, normalized by the end-use intensity of energy class level G [72] (assumed $E_{reference}$), equal to 380 kWh/m^2/year for residential buildings in The Netherlands. The RR_{Rec} was computed considering two weeks after the heatwave as a reference period. $T_{SET\,crit}$ defined the hours returning to SET 30 °C by the two-week recovery period. E_{Rec} measured the cooling energy consumption during recovery using the same threshold as E_{Res} ($E_{reference}$), with only the reference period changing.

The final *RR* values were calculated by assigning a 50/50 wt (w_{Resi} and w_{Reci} exponents in Eqs. (1) and (2)) to the indicators in the response and recovery phase, while a 100/0 wt (w_{Res}/ w_{Rec}) was applied to the RR_{Res}/RR_{Rec} (Eq. (3)), due to the negligible recovery time observed after the event. This was because, as outdoor temperatures dropped immediately after the heatwave, the indoor SET had already fallen below 30 °C by the time the heatwave ended. The final *RR* values ranged from 0.67 to 0.77 for all the buildings (Table 3),

Table 2
Building archetypes in the Amsterdam urban block.

	Archetype 1	Archetype 2	Archetype 3	Archetype 4	Archetype 5	Archetype 6
Construction year	<1975	>1995	<1975	<1975	>1995	<1975
Building use	Domestic	Domestic	Domestic	Mixed-use	Mixed-use	Retail
Air Conditioner Use	No	Yes	No	No	Yes	Yes
Wall type	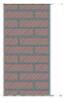 Load-bearing masonry	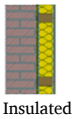 Insulated load-bearing masonry	 Load-bearing masonry	 Load-bearing masonry	 Insulated load-bearing masonry	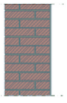 Load-bearing masonry
R-value wall [W/m^{2}K]	0.35	2.5	0.35	0.35	2.5	0.35
U-value windows [W/m^{2}K]	5.8	1.1	5.8	5.8	1.1	5.8
Window-to-Wall Ratio	0.45	0.45	0.49	0.45	0.45	0.39
R-value roof [W/m^{2}K]	0.35	2.5	0.35	0.35	2.5	0.35
R-value floor [W/m^{2}K]	0.15	2.5	0.15	0.15	2.5	0.15
Infiltration ratio [m^3/s per m^2 façade]	0.0007	0.0004	0.0007	0.0007	0.0004	0.0007

Note. U-value indicates thermal transmittance; R-value denotes thermal resistance.

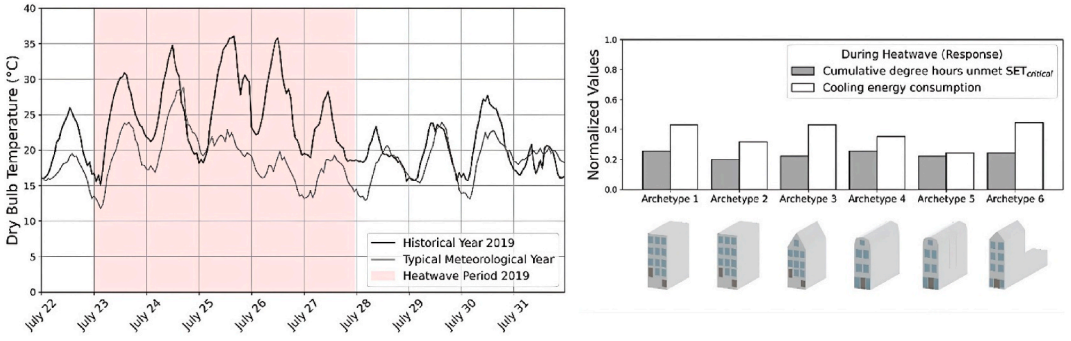

(a) (b)

Fig. 6. (a) Historical (July 2019) vs. TMY weather data for Amsterdam. (b) Heat resilience indicators (response: $CDH_{SET\,crit}$, E_{Res}) for the buildings in Amsterdam.

indicating resilience ratings in classes B and A, respectively. Comparisons between archetypes revealed the influence of construction layers and shape geometry on the *RR* values. Archetypes 2 and 5 resulted in the highest values, as these buildings - constructed after 1995 - have lightweight cladding with high thermal resistance (low thermal transmittance) compared to ones with masonry walls. For archetypes with similar E_{Res} values, further comparisons of E_{Res} revealed that buildings with lower compactness ratios tended to have lower energy consumption. It is important to note that this study did not account for the heat island effect, which could have raised outdoor temperatures and potentially resulted in lower resilience levels. The choice of a lower discomfort threshold levels, particularly depending on occupant sensitivity, could also contribute to this increase.

To further evaluate the influence of weight selection on the final outcomes, a sensitivity analysis was conducted. When varying the weights assigned to the two factors ($CDH_{SET\,crit}$, E_{Res}) within the response phase - combined into a geometric aggregation (Eq. (1)) - a limited variation is observed across all buildings. Greater sensitivity appears in buildings with lower resilience indicators, where values ranged from 0.56 to 0.74 when shifting between the "extreme" weightings of 0/100 and 100/0, that is, assigning full weight to one factor over the other (Fig. 7a). In contrast, more pronounced variability was observed when adjusting the weights between the two resilience phases (RR_{Res}, RR_{Rec}), which led to changes in the final resilience classification. This sensitivity is primarily driven by the strong influence of the response phase, with up to two or four resilience class shifts occurring when moving from a 0/100 to 100/0 weighting for RR_{Res}/RR_{Rec} (Fig. 7b), further highlighting how weights selection can impact the final resilience score. In the specific case study, recovery indicators were found to be negligible; therefore, a 100/0 weighting favoring the response phase was adopted, resulting in more conservative (i.e., lower) resilience scores.

3.2. The Acerra case study

An urban block in Acerra, Campania region (Italy), was chosen due to the area's high vulnerability to climate-induced events. In particular, in 2022 the region experienced a 35 % increase in extreme events compared to the previous year, including intense heatwaves [73]. The region is also potentially affected by moderate-intensity earthquakes. Therefore, both climate-induced (heat, flood, wind) and seismic hazards were considered in this application. This choice also aligns with the current need for a national plan for reducing these risks and advancing integrated rehabilitation of the building stock [74]. The selected area in Acerra features residential buildings constructed in the 1980s featuring similar construction systems and materials (Table 4), but different geometries (number of stories, floor area, compactness ratio) (Fig. 8, Table 5).

Heatwave data acquisition and building energy simulations for the heat resilience assessment followed the same approach used in the Amsterdam case study. Daily climate observations from Naples Capodichino airport weather station for 1951–2023 were obtained from the Open-Meteo database [75]. Using the CTX90pct criterion, August 8–15-2021 was identified as the heatwave with the highest maximum daily temperature (36.9 °C). Fig. 9a shows the hourly dry bulb temperature during the 2021 heatwave period alongside the TMY. During the 2021 heatwave, temperatures were up to 7 °C higher than the typical year. After the heatwave, temperatures for both years aligned, with values remaining above 30 °C.

Using this historical heatwave, energy simulations were conducted for the 19 buildings of the area. When calculating the RR_{Heat}

Table 3
Heat resilience scoring per building archetype in the Amsterdam urban block.

Archetype	1	2	3	4	5	6
RR	0.70	0.77	0.67	0.67	0.75	0.69
RRL class	B	A	B	B	B	B
Rank	3	1	5	6	2	4

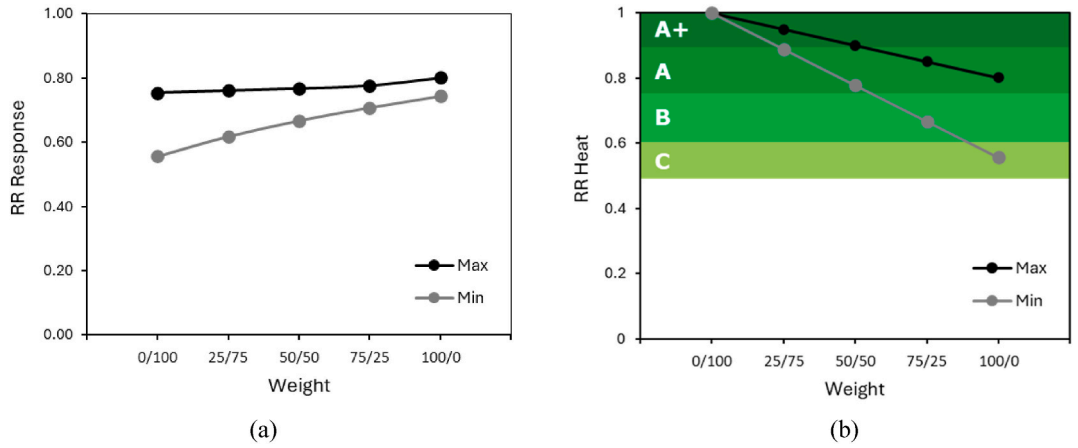

Fig. 7. (a) Variation of RR_{Res} (max and min values from all buildings) as a function of the weights assigned to $CDH_{SET\,crit}/E_{Res}$; b) Variation of RR_{Heat} (max and min values from all buildings) as a function of the weights assigned to RR_{Res}/RR_{Rec}.

Table 4
Building archetype in the Acerra urban block.

		Structure		Façade			
Construction year	Building Use	Material	Lateral force-resisting system	Wall	Windows	Floor	Roof
1980	Domestic	Reinforced Concrete Frame	Masonry-Infilled frames	Hollow brick masonry (R-value: 0.99 W/m^{2}K)	Single pane, wood frame (U-value: 4.36 W/m^{2}K)	Reinforced brick-concrete slab (R-value: 0.47 W/m^{2}K)	Reinforced brick-concrete slab (R-value: 0.56 W/m^{2}K)

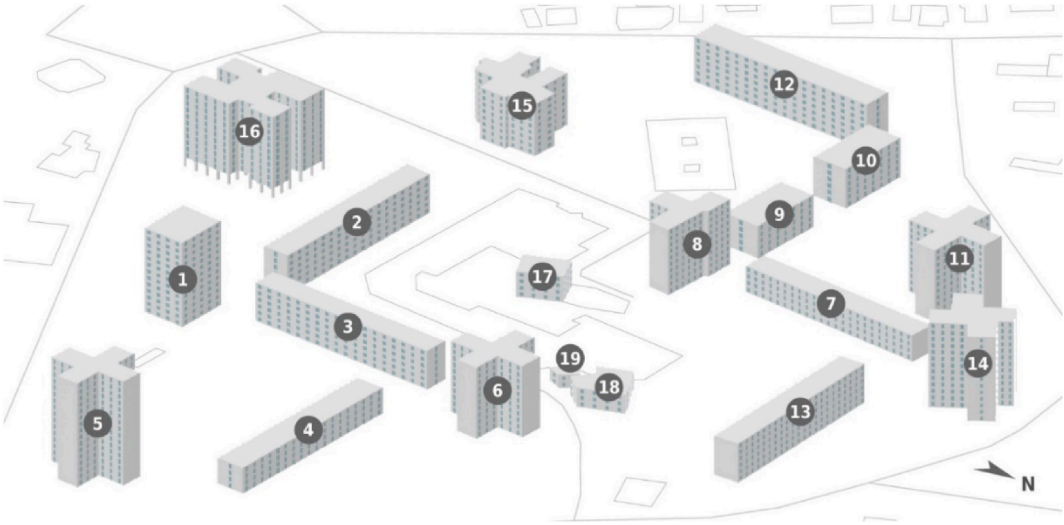

Fig. 8. Isometric perspective of the urban block analyzed in Acerra, with index numbers indicating the buildings in Table 5.

values, the same resilience indicators ($CDH_{SET\,crit}, E_{Res}$; $T_{SET\,crit}, E_{Rec}$) and approach as the Amsterdam case study were considered. The only difference was the reference value used to normalize energy consumption, set at 400 kWh/m^2/year for Acerra, based on a class G level for residential buildings in Italy [76]. Fig. 9b shows the heat resilience indicators during and after the heatwave for all buildings. $CDH_{SET\,crit}$ and $T_{SET\,crit}$ values indicate the worst conditions for the response and recovery phases respectively, with no clear common pattern of SET emerging, while the cooling energy consumption show similar trends in the response and recovery phases. Assuming equal importance for response/recovery (w_{Res}/ w_{Rec} = 50/50), the RR_{Heat} values were derived, ranging from 0.35 to 0.50 for all buildings and indicating heat resilience ratings in classes E and D (Table 6). This lower resilience score, compared to the Amsterdam

Table 5
Geometric characteristics per building in the Acerra urban block.

Building	1	2	3	4	5	6	7	8	9	10	11	12	13	14	15	16	17	18	19
Number of Floors	13	6	6	4	16	11	4	10	5	6	11	7	6	13	8	12	4	3	2
Compactness Ratio	0.25	0.36	0.34	0.37	0.29	0.31	0.39	0.32	0.34	0.31	0.30	0.29	0.36	0.27	0.34	0.24	0.45	0.48	0.91
Total Floor Area $[m^2]$	5384	5742	5152	3880	8458	5784	3515	4387	2550	2954	6467	7344	5095	7801	5742	10945	977	982	112

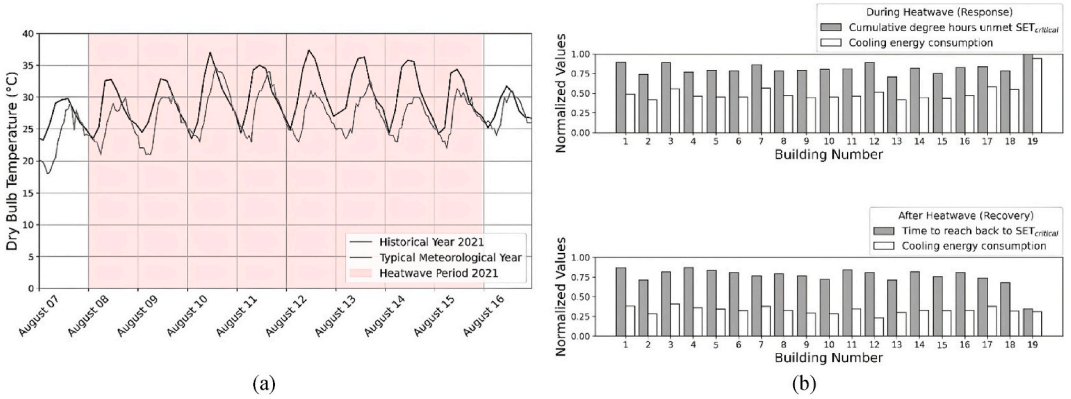

Fig. 9. (a) Historical (August 2021) vs. TMY weather data for Acerra. (b) Heat resilience indicators (response: $CDH_{SET\,crit}$, E_{Res}; recovery: $T_{SET\,crit}$, E_{Rec}) for the buildings in Acerra.

case study, suggests that the buildings are less prepared for extreme heat. A comparison of *RR* values across all buildings shows that those with lower compactness ratios generally exhibit higher resilience; this is likely due to their reduced exposed surface areas, which absorb and retain less heat. For example, Building 2 has a compactness ratio of 0.36 and ranks 1st in resilience ($RR = 0.50$, Class D), while Building 19 has the highest compactness ratio (0.91) and ranks last ($RR = 0.35$, Class E). Mid-rise buildings (4–8 floors) tend to perform better in heat resilience than low-rise (1–3 floors) or high-rise buildings (10+ floors). There is no clear trend between total floor area and resilience, indicating that other geometric factors (compactness and height) play a more significant role.

Based on stakeholder priorities and the need to address all resilience domains (see Table 1), seismic resilience was assessed using four key indicators: (i) $MAFE_E$ (for the collapse limit state) and repair costs RC_E to define the response phase (RR_{Res}); (ii) DT_E downtime and CE_E carbon emissions for the recovery phase (RR_{Rec}). *MAFE* was calculated following the methodology proposed by Iervolino et al. [77]. The other loss-related indicators were assessed using the Performance-Based Earthquake Engineering (PBEE) [78] methodology. Seismic hazard data was sourced from the MPS04 seismic hazard model [79], adjusted for B soil type [80] (Fig. 10a). Vulnerability models specific to the Italian building stock were derived from Aljawhari et al. [81], categorizing buildings by the number of floors and year of construction (thus leading to three classes: Low, Mid and High rise buildings). The buildings in Acerra, constructed after the city was designated a seismic zone in 1981 [82], were designed with some consideration of seismic actions (low-code level), though they lack the detailed seismic provisions mandated by more modern seismic codes.

The computed resilience indicators were normalized as indicated in Table 1. As discussed in Section 2.2, the obtained values were remapped using a logistic logarithmic function for their use in the multi-criteria decision making approach. The mean (μ) and standard deviation (β) parameters of this function, can be defined by stakeholders to align with their risk profile and what they deem unacceptable. In this specific application, *MAFE* normalization used the minimum target (mean value of $2 \cdot 10e\text{-}4$) for new buildings as outlined by Franchin & Noto [57], with a 0.6 dispersion value, while a 0.15 % mean was applied for annual repair costs, downtime and carbon losses as acceptable risk level, with a 0.4 dispersion value. The dispersion values were based on damage state and consequence functions variability as defined in the FEMA P-58 [16].

The normalized indicators for all buildings (Fig. 10b) reveal that repair costs have higher impact on the response phase, resulting in a final RR_{Res} in the range of 0.45–0.72 (using 0.5 weighting in the sub-index). In the recovery phase, normalized carbon emissions are slightly higher than downtime, leading to RR_{Rec} values between 0.28 and 0.67. This indicates that the buildings are better prepared for the response phase compared to the recovery phase. Following the same approach used for heat resilience – where equal importance is assumed for response/recovery ($w_{Res}/\ w_{Rec} = 50/50$), the $RR_{Seismic}$ values were derived and are summarized in Table 7. Since the buildings were constructed in the same period and the only difference is the number of stories, the results are obtained for the three analyzed categories: high-rise buildings exhibit lower resilience values (RRL = E), mid-rise buildings show an RRL = D, and higher resilience is observed in low-rise buildings (RRL = B). This classification is also a result of combining the vulnerability models with the seismic hazard specific to each building class (Fig. 10a). It is observed that the archetype-based seismic assessment, used in this preliminary analysis of the area, does not allow for defining a hierarchy of resilience levels among buildings within the same class, whereas a more detailed numerical analysis could help in this regard.

The risk posed by synoptic winds was also assessed to include its effects into the multi-hazard resilience rating. The hazard was determined based on the CNR-DT guidelines [83], which provide criteria for defining wind loads on structures. The vulnerability model assumed for the buildings was the one proposed by Feuerstein et al. [84] for concrete structures, also adopted in the European wind damage assessment by Koks & Haer [85]. However, after integrating hazard and vulnerability, the wind consequences were determined to be negligible - for example, the EAL was found to be below 10^{-6}. Consequently, wind hazard was deemed immaterial for the case study area.

Finally, flood risk was assessed for the Acerra urban block. Given the distance from both the coast and major rivers, pluvial flooding was identified as the primary hazard. Flood resilience was evaluated using four key indicators: (i) water depth *WD*, relative to the 100 years of return period (as per ASCE standard [56] for ordinary structures), and repair costs RC_F to define the response phase (RR_{Res}); (ii)

Table 6
Heat resilience scoring for the buildings in the Acerra urban block.

Building	1	2	3	4	5	6	7	8	9	10	11	12	13	14	15	16	17	18	19
RR	0.38	0.50	0.36	0.42	0.43	0.45	0.38	0.44	0.46	0.47	0.42	0.45	0.50	0.44	0.47	0.43	0.39	0.44	0.35
RRL	D	D	E	D	D	D	D	D	D	D	D	D	D	D	D	D	D	D	E

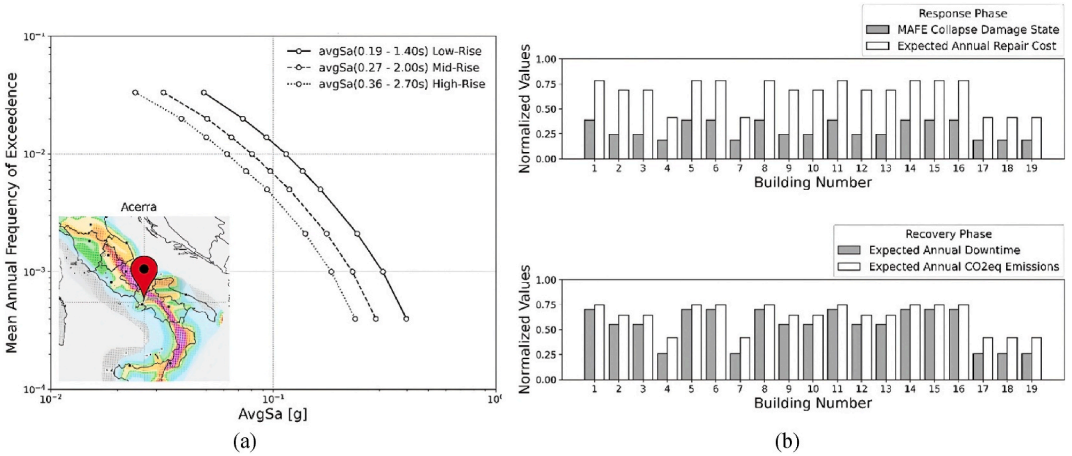

Fig. 10. (a) Seismic hazard curves for the Acerra region (Mean Annual Frequency of Exceedance vs. Average Spectral Acceleration -AvgSa - for Low, Mid and High rise buildings). (b) Seismic resilience indicators for the buildings in Acerra.

DT_F downtime and CE_F carbon emissions for the recovery phase (RR_{Rec}). The hazard data for the case study area was sourced from Fathom Global model [86] for multiple return periods, considering a RCP 8.5 climate scenario for the year 2050 (Fig. 11a). For each building, the hazard curve was defined as the maximum flood elevation expected across the building footprint (Fig. 11b). Vulnerability models were derived from a component-based loss assessment of a representative building archetype, as described by REDi Flood Guidelines [13], i.e., a four-story building without a basement. Building components were based on the FEMA P-58 [16] normative quantities for a residential building. The vulnerability model, for repair costs and carbon emissions, was scaled according to the number of floors of the building in the case study area relative to the archetype, under the assumption that only the first floor (i.e. ground floor) is affected by flooding. Another key assumption was the use of flood depth as the engineering demand parameter, while neglecting the effect of flow velocity. This simplification was deemed acceptable due to the nature of the hazard (i.e., pluvial flooding). A uniform first-floor elevation of 10 cm was assumed for all buildings, and this value was considered in the normalization of the water depth *WD*. Impeding factors were not considered in the evaluation of downtime for consistency with the seismic hazard. The water depth corresponding to the 100-year return period was found to be zero for all buildings in the study area. Even under the 1000-year return period scenario, only five buildings were affected by flooding. Estimates of RC_F, DT_F and CE_F were computed and normalized following the same approach adopted for the seismic analysis. Renormalization using a logistic function was conducted with identical parameters to ensure consistency. The results indicate that flood risk is primarily driven by the hazard intensity and the number of building floors. Notably, the hazard exhibits non-zero values only for return periods exceeding 200 years. Moreover, taller buildings exhibit lower loss values, as flooding affects only the first (ground) floor while losses are normalized against the value of the entire structure. When computing the resilience indicators, resilience losses were therefore found to be almost zero for all buildings. As a result, both the response and recovery capacity for flood hazard equaled 0.99–1.00 across all buildings. This outcome is attributed to the use of indicators that represent annualized values derived from a time-based assessment (as discussed in Section 2.1). A scenario-based approach - such as selecting a 1000-year return period flood event - could have yielded a different result in the resilience quantification.

Finally, the obtained $RR_{Res/Rec}$ values for heat, seismic and flood resilience are combined to derive multi-hazard resilience scores as indicated in Section 2.4. Assigning equal importance for response and recovery to all hazards and applying the TOPSIS method, the final resilience levels (C_i^*) were derived and the buildings were classified in terms of *RRL* (Table 8, Fig. 12). This ranking provides an integrated assessment of the area, useful for an initial prioritization of integrated retrofitting strategies. The results highlight that low-rise buildings tend to exhibit higher resilience scores, particularly in seismic scenarios, with RR_{Res-E} reaching a maximum of 0.72 and RR_{Rec-E} up to 0.67. This higher performance can be attributed to their reduced mass and typically more favourable compactness ratios, which also support passive thermal performance. However, they show greater variability in heat resilience, with RR_{Res-H} ranging from 0.03 to 0.40, indicating less consistent performance in overheating conditions. Mid-rise buildings demonstrate moderate and relatively balanced resilience across both hazards, with RR_{Res-H} ranging from 0.29 to 0.46 and RR_{Res-E} from 0.40 to 0.59. This suggests that these buildings may benefit from a balance between structural stability and thermal performance, although their increased height may introduce vulnerability under seismic loading. The narrower range of recovery scores also indicates more predictable post-event performance. High-rise buildings show the lowest resilience values, especially in the seismic domain ($RR_{Res-E} = 0.45$, $RR_{Rec-E} = 0.28$). These buildings often have increased dynamic response during earthquakes and higher internal loads during heatwaves, contributing to greater energy use and longer recovery periods. Although they exhibit slightly more consistent performance in thermal resilience ($RR_{Res-H} = 0.34$–0.42), their overall lower scores indicate increased vulnerability due to height and system complexity, especially when compactness is low or envelope design is suboptimal. As discussed above, RR_{Res-F} and RR_{Rec-F} are equal to 0.99–1.00 for all buildings, therefore flood hazard is not impacting the final resilience scoring (Table 8), particularly in the determination of the total ideal (S_i^+) and negative ideal solution (S_i^-) (Eq. (4)).

Table 7
Seismic resilience scoring for the buildings in the Acerra urban block.

Building	1	2	3	4	5	6	7	8	9	10	11	12	13	14	15	16	17	18	19
RR	0.36	0.50	0.50	0.70	0.36	0.36	0.70	0.36	0.50	0.50	0.36	0.50	0.50	0.36	0.36	0.36	0.70	0.70	0.70
RRL	E	D	D	B	E	E	B	E	D	D	E	D	D	E	E	E	B	B	B

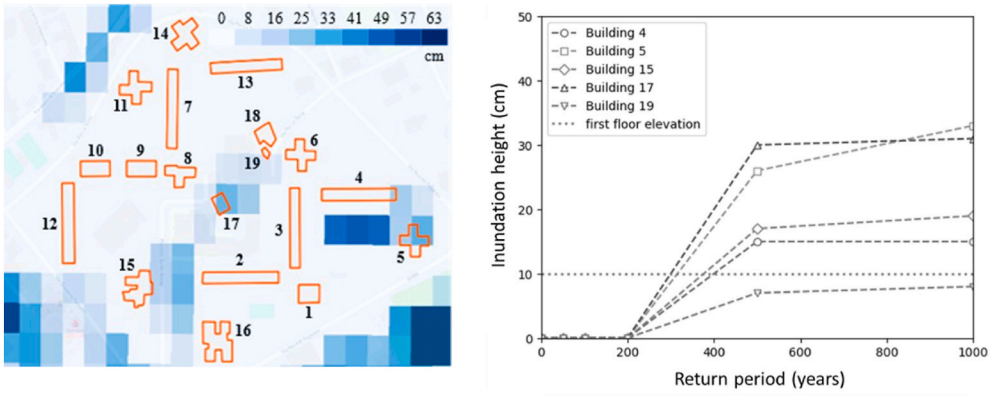

Fig. 11. (a) Flood hazard map for the Acerra region (Pluvial flooding - RCP 8.5 for year 2050, 50th Percentile - 1000 years return period) overlayed on the case study buildings (highlighted in orange). (b) Flood hazard curves for affected buildings in the Acerra urban block.

Among all the buildings, the results indicate that Building 18 has the highest resilience value, due to its relatively low number of floors (3) and a compactness ratio of 0.48. Building 1's relatively poor resilience (RRL = E) can be attributed to its height (13 floors), which increases vulnerability in both heat and seismic conditions. Although its compactness ratio is low, which might help with heat resilience to some extent, its large size make it less resilient compared to mid-rise or low-rise buildings, and its seismic vulnerability especially affects the multi-hazard resilience score.

When comparing single-hazard to multi-hazard resilience scores, it is evident that heat resilience has a greater impact during the response phase, whereas seismic resilience plays a more significant role in the recovery phase. The rankings of buildings change when considering both hazards simultaneously, as the relative rankings adjust to provide a more balanced assessment of building integrated performance across multiple factors. It is however observed that buildings with low-rise designs typically dominate the top ranks, owing to their better overall performance in both heat and seismic conditions.

As an extension of the previous analysis, a further study was conducted to assess the impact of weight assignment on the final resilience scores. In this case, weights were derived using the AHP, which involved pairwise comparisons between all RR_{Res} and RR_{Rec} values across the three considered hazards, resulting in a total of six criteria. *Case 1* in Fig. 13 represents the baseline scenario, in which equal importance is assumed for all criteria, assigning a uniform weight of 0.167 to each. In addition to this baseline, two alternative decision-making scenarios were evaluated. In *Case 2*, greater importance is assigned to heat resilience, with weights of 0.322 for RR_{Res-H} and RR_{Rec-H}, 0.141 for RR_{Res-E} and RR_{Res-E}, 0.037 for RR_{Res-F} and RR_{Res-F}. Under this configuration, low-rise buildings (Buildings 4, 7, 17–19) experienced a moderate decrease in resilience scores (approximately 10–20 %), while mid-to high-rise buildings showed a significant increase (20–35 %). Conversely, in *Case 3*, seismic resilience is prioritized with weights of 0.322 for RR_{Res-E} and RR_{Rec-E}, 0.141 for RR_{Res-H} and RR_{Res-H}, 0.037 for RR_{Res-F} and RR_{Res-F}. In this scenario, low-rise buildings saw an increase in resilience (10–30 %), while mid-to high-rise buildings experienced a notable decrease (10–40 %). These results clearly demonstrate how the final resilience scores are directly influenced by the weight selection process, highlighting that mid- and high-rise buildings are particularly sensitive to changes in seismic resilience weights, which could be prioritized in this specific multi-hazard application.

4. Final remarks

To-date, standardized methods and frameworks for resilience assessment are unavailable, but they are essential if designers, owners and decision-makers attempt to holistically address the impact of climate change and other extreme events. The proposed resilience indicators, indices and rating scheme represent an initial effort towards this need. As demonstrated in the case study applications, this index-based approach is useful for comparing the holistic resilience of buildings and for quantifying the impacts of future single or multiple threats. The resilience value can be used to rank buildings and determine whether their resilience levels meet acceptable standards based on local policies. In Amsterdam, for instance, this could involve aligning with the requirements outlined in the under-development Heat Program by the municipality, as the current initiatives only concern heating solutions in winter [87]. The ranking can also support effective resource allocation by enabling preliminary prioritization of interventions or identifying buildings that require more detailed investigations, as for the Acerra case study. However, it is worth noting that the analyzed urban blocks primarily focused on residential buildings, and incorporating additional importance factors could enhance prioritization particularly when different building uses are considered within a specific area.

The implementation of a resilience readiness framework could also support the introduction of dedicated incentives for integrating resilient technologies into buildings and promote technological innovation in construction. Resilience indicators and/or holistic indices can be incorporated into early-stage building design to guide the selection of rehabilitation/retrofit or design options for a specific building project, enabling the identification of enhanced solutions with the highest resilience value. However, it is important to note that the choice of normalization thresholds significantly impacts the results and should be tailored to local conditions and

Table 8
Multi-hazard resilience scoring for the buildings in the Acerra urban block.

Building	1	2	3	4	5	6	7	8	9	10	11	12	13	14	15	16	17	18	19
C_i^* value	0.36	0.60	0.44	0.72	0.41	0.43	0.68	0.42	0.56	0.57	0.41	0.53	0.60	0.42	0.44	0.40	0.69	0.77	0.56
RRL	E	C	D	B	D	D	B	D	C	C	D	C	C	D	D	D	B	A	C
Rank	19	6	12	2	16	13	4	14	8	7	17	10	5	15	11	18	3	1	9

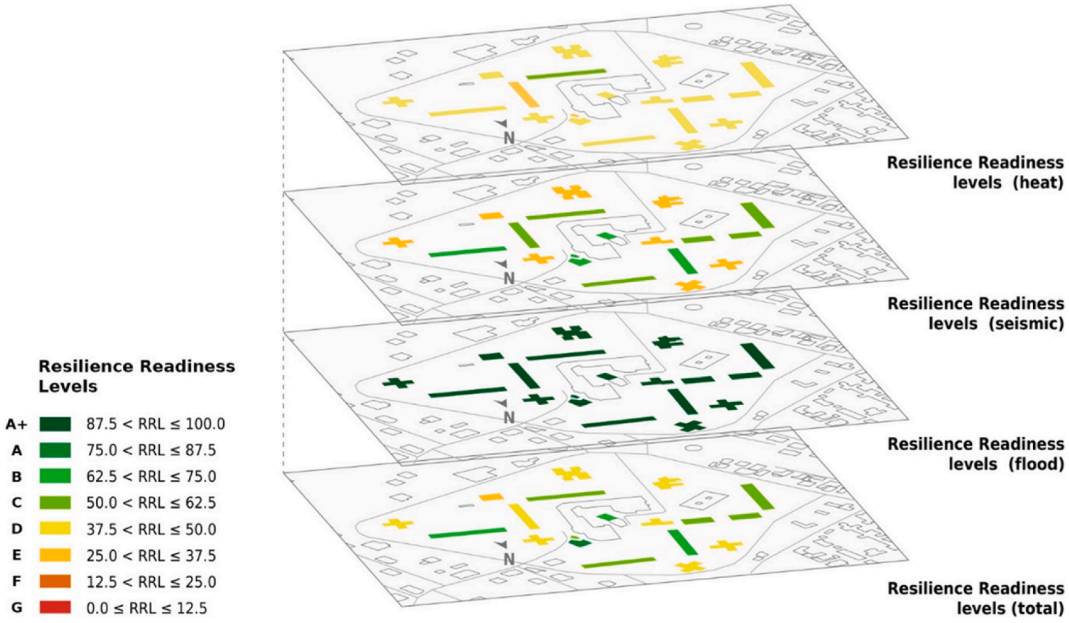

Fig. 12. Multi-hazard resilience map for the Acerra urban block.

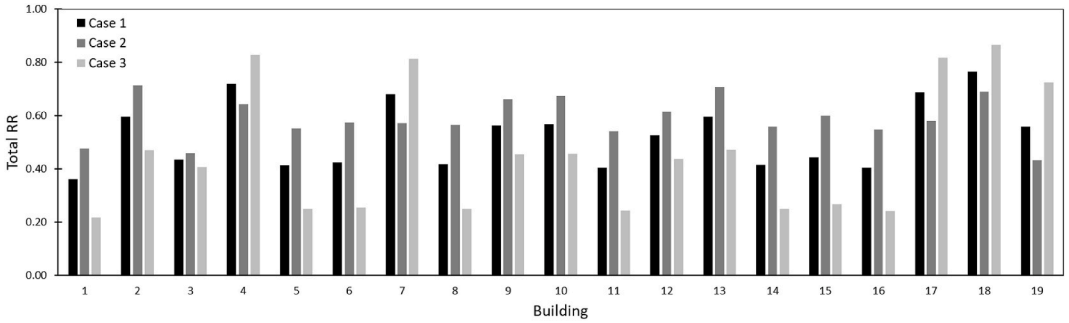

Fig. 13. Variation of the multi-hazard resilience score considering different weights: *Case 1* - all hazards are equally important; *Case 2* - Heat is moderately more important than Seismic and very strongly more important than Flood, while Seismic is strongly more important than Flood; *Case 3* - Seismic is moderately more important than Heat and very strongly more important than Flood, Heat is strongly more important than Flood.

project constraints. For instance, in the case studies, SET was based on the critical threshold for unliveable conditions; using a lower discomfort threshold would result in lower resilience ratings.

The proposed approach allows resilience indicators to be derived using either simplified (analytical/empirical) methods or more detailed numerical analyses. For rapid resilience assessments, performance values can be obtained using analytical calculations or fragility data of building archetypes (e.g., seismic assessment for Acerra). This approach evaluates the impact of historical events and potential hazard scenarios over a building's lifetime, supporting insurance and reinsurance sectors that typically assess the consequences of 'worst-case' or 'most probable' scenarios. In addition to simplified assessments, resilience indicators can be calculated through refined numerical simulations. This involves defining hazard models and implementing finite element models to conduct either quasi-deterministic, scenario or intensity-based, performance assessments (e.g., energy simulations for both Amsterdam and Acerra) or probabilistic component-level assessment accounting for all possible uncertainty sources (hazard-related, building definition and knowledge, occupants, consequences, threshold values). This flexibility allows to accommodate different levels of risk assessment, ranging from basic archetype evaluations to advanced component-level assessments [88] (Fig. 14), highlighting the potential to extend the approach to multi-scale assessments.

While the present study does not explicitly model regional variations, the proposed framework is inherently flexible and capable of incorporating them. For example: (i) the estimation of expected annual losses uses hazard- and building-specific parameters that can be adjusted to reflect local conditions (e.g., region-specific hazard priorities or exposure patterns); (ii) variables such as total replacement and recovery time can be adapted to account for local impeding factors - such as material availability or regulatory constraints; (iii) the AHP-based weighting system can be customized using expert judgment or empirical data, ensuring that it reflects the priorities and risk perceptions relevant to a specific region.

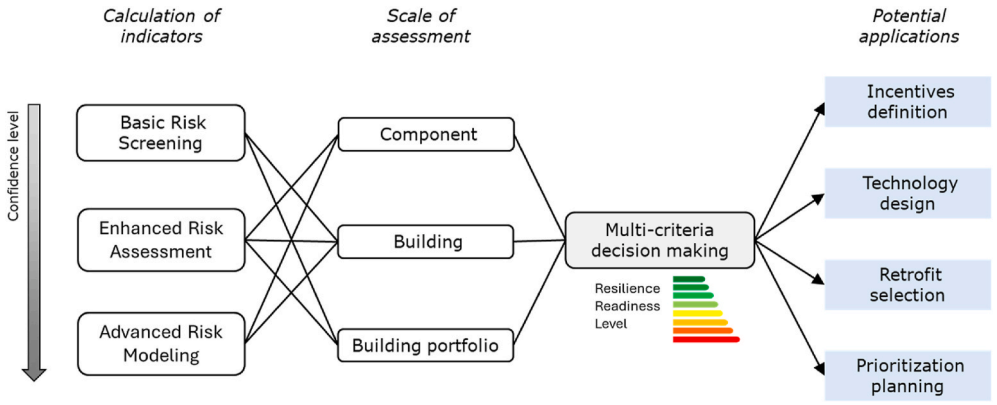

Fig. 14. Applicability of the proposed resilience index and Resilience Readiness Levels.

The approach also offers flexibility in data acquisition. When data availability or quality is limited - particularly for component-level risk assessments - a knowledge-based approach can be used to derive ranges of *RRL* values rather than a single score, which can be progressively refined as more data become available [89]. However, the approach may encounter limitations in large-scale applications, where data aggregation can obscure important local variations and lead to less accurate resilience estimates. Further investigation is needed for such cases, as aggregated scoring may mask critical differences that a single consolidated value cannot capture. Additionally, at broader spatial scales, aggregation introduces greater uncertainty and requires a careful balance between geospatial resolution and computational efficiency to support disaster and emergency preparedness. To address these challenges, a hybrid approach - combining both aggregated and disaggregated results - is recommended as a versatile and more robust solution.

5. Conclusions

As environmental uncertainties increase, there is an urgent need for holistic resilience assessment of buildings, particularly in an urban environment. The multifaceted nature of resilience requires multi-criteria indicators and calculation methods for both single-hazard and multi-hazard scenarios. This study addresses this need by providing a set of comprehensive indicators, that encompass structural safety, energy efficiency, carbon emissions, occupant well-being and cost, and establishes resilience readiness levels for buildings. These indices evaluate the effectiveness of buildings to respond to and recover from diverse extreme events. To aid decision-makers in evaluating and comparing resilience across different risk scenarios, the study also introduces a resilience rating system. The approach was demonstrated on urban blocks in The Netherlands and Italy, which are exposed to different hazards and climates. The demonstration showed the adaptability of the proposed method across varying environmental conditions and diverse contexts.

The paper has provided a practical framework to assess the resilience of buildings and inform decision-making and multi-risk management. The approach was initially conceived and demonstrated for urban block assessments, but it is adaptable to various levels of refinement, ranging from archetype-specific to component-level analyses. As a result, it can be extended to incorporate additional hazards and assess resilience across different scales, from individual building subsystems (e.g., structure or facades) to entire neighborhoods. The current methodology is designed to evaluate hazards independently, aligning with common practice in the field; however, interdependencies between hazards can impact resilience outcomes, suggesting that the framework could be extended to address multi-hazard scenarios. Furthermore, interdependencies between resilience indicators are not currently accounted for, but could be addressed in future developments - for example, through the introduction of coupling indicators that represent the combined effects of two or more underlying indicators. Although expert-driven weighting involves some subjectivity, applying consistency checks and sensitivity analyses can improve transparency and reduce its impact. Future work could develop weighting matrices based on policies and stakeholder input, tailored to specific hazards and building types, to ensure consistent and context-appropriate weight definitions. Finally, as a further development, the proposed multi-domain indicators could be used to set resilience-based design objectives tailored to a building's use and hazard exposure. This involves defining resilience goals for risk categorization, functionality and recovery, enhancing both design and retrofitting efforts.

CRediT authorship contribution statement

Simona Bianchi: Writing – review & editing, Writing – original draft, Visualization, Supervision, Methodology, Funding acquisition, Conceptualization. **Michele Matteoni:** Writing – original draft, Visualization, Methodology, Investigation. **Kyujin Kim:** Writing – original draft, Visualization, Methodology, Investigation. **Anna Maria Koniari:** Writing – original draft, Visualization, Methodology, Investigation. **Kyra Koning:** Writing – original draft, Visualization, Investigation. **Romulus Costache:** Writing – review & editing, Methodology. **Nicu Ciobotaru:** Writing – review & editing, Methodology. **Alessandra Luna-Navarro:** Writing – review & editing, Supervision. **Zhikai Peng:** Writing – review & editing. **Jonathan Ciurlanti:** Writing – review & editing, Supervision. **Hamidreza Shahriari:** Writing – review & editing. **Divyae Mittal:** Writing – review & editing. **Evdokia Stavridou:** Writing – review

& editing. **Anna Silva:** Writing – review & editing. **Michele Palmieri:** Writing – review & editing. **Stefano Pampanin:** Writing – review & editing. **Francesco Petrini:** Writing – review & editing, Supervision. **Mauro Overend:** Writing – review & editing.

Declaration of competing interest

The authors declare that they have no known competing financial interests or personal relationships that could have appeared to influence the work reported in this paper.

Acknowledgements

This study has received funding from the European Union under the Horizon Europe Research & Innovation Programme (Grant Agreement no. 101123467 MULTICARE - Multi-hazard low-carbon resilient technologies and multi-scale digital services for a future-proof, sustainable & user-centred built environment).

Data availability

Data will be made available on request.

References

[1] European Environment Agency, Economic losses from weather- & climate-related extremes in Europe. eea.europa.eu/en/analysis/indicators/economic-losses-from-climate-related, 2024.
[2] J. Ballester, et al., Heat-related mortality in Europe during the summer of 2022, Nat. Med. 29 (2023) 1857–1866, https://doi.org/10.1038/s41591-023-02419-z.
[3] D. García-León, et al., Temperature-related mortality burden and projected change in 1368 European regions: a modelling study, Lancet (2024), https://doi.org/10.1016/S2468-2667(24)00179-8.
[4] European Commission, Buildings and construction. europa.eu/industry/sustainability/buildings-and-construction_en, 2022.
[5] C.I. Donatti, et al., Global hotspots of climate-related disasters, Int. J. Disaster Risk Reduct. 108 (2024) 104488, https://doi.org/10.1016/j.ijdrr.2024.104488.
[6] EM-DAT, The international disaster database, centre for research on the epidemiology of disasters. public.emdat.be/, 2024.
[7] S. Hosseini, K. Barker, J.E. Ramirez-Marquez, A review of definitions and measures of system resilience, Reliab. Eng. Syst. Saf. 145 (2016) 47–61, https://doi.org/10.1016/j.ress.2015.08.006.
[8] S. Argyroudis, et al., Resilience assessment framework for critical infrastructure in a multi-hazard environment: case study on transport assets, Sci. Total Environ. 714 (2020) 136854, https://doi.org/10.1016/j.scitotenv.2020.136854.
[9] G. Cremen, C. Galasso, J. McCloskey, Modelling and quantifying tomorrow's risks from natural hazards, Sci. Total Environ. 817 (2022) 152552, https://doi.org/10.1016/j.scitotenv.2021.152552.
[10] F. Laurien, J.G.C. Martin, S. Mehryar, Climate and disaster resilience measurement: persistent gaps in multiple hazards, methods, and practicability, Clim. Risk Manag. 37 (2022) 100443, https://doi.org/10.1016/j.crm.2022.100443.
[11] S. Hochrainer-Stigler, et al., Toward a framework for systemic multi-hazard and multi-risk assessment and management, iScience 26 (2023) 103736, https://doi.org/10.1016/j.isci.2023.106736.
[12] I. Almufti, M. Willford, Redi™ Rating System: Resilience-Based Earthquake Design Initiative for the next Generation of Buildings, 2014, https://doi.org/10.13140/RG.2.2.20267.75043.
[13] J. Hogan, I. Almufti, M. Ackerson, Redi™: Resilience-Based Design Guidelines for Floods, Arup, 2023.
[14] I. Almufti, J. Hogan, A. Leitch, H. Rosenberg, Redi™: Resilience-Based Design Guidelines for Extreme Windstorms, Arup, 2023.
[15] M. Bruneau, et al., A framework to quantitatively assess and enhance the seismic resilience of communities, Earthq. Spectra 19 (2003) 733–752, https://doi.org/10.1193/1.1623.
[16] FEMA, Seismic Performance Assessment of Buildings, Volume 1 – Methodology, 2018. Washington D. C., USA, femap58.atcouncil.org/reports.
[17] V. Silva, et al., Current challenges and future trends in analytical fragility and vulnerability modeling, Earthq. Spectra 35 (2019) 1927–1952, https://doi.org/10.1193/042418EQS101O.
[18] A.H. Herbin, M. Barbato, Fragility curves for building envelope components subject to windborne debris impact, J. Wind Eng. Ind. Aerod. 107–108 (2012) 285–298, https://doi.org/10.1016/j.jweia.2012.05.005.
[19] O.M. Nofal, J.W. van de Lindt, T.Q. Do, Multi-variate and single-variable flood fragility and loss approaches for buildings, Reliab. Eng. Syst. Saf. 202 (2020) 106971, https://doi.org/10.1016/j.ress.2020.106971.
[20] F. Biondini, E. Camnasio, A. Titi, Seismic resilience of concrete structures under corrosion, Earthq. Eng. Struct. Dynam. 44 (2015) 2445–2466, https://doi.org/10.1002/eqe.2591.
[21] Y. Dong, D.M. Frangopol, Probabilistic time-dependent multihazard life-cycle assessment and resilience of bridges considering climate change, J. Perform. Constr. Facil. 30 (2016) 5, https://doi.org/10.1061/(ASCE)CF.1943-5509.0000883.
[22] S. Homaei, M. Hamdy, Thermal resilient buildings: how to be quantified? A novel benchmarking framework and labelling metric, Build. Environ. 201 (2021) 108022, https://doi.org/10.1016/j.buildenv.2021.108022.
[23] S. Attia, et al., Resilient cooling of buildings to protect against heat waves and power outages: key concepts and definition, Energy Build. 239 (2021) 110869, https://doi.org/10.1016/j.enbuild.2021.110869.
[24] D. Amaripadath, P.A. Mirzaei, S. Attia, Multi-criteria thermal resilience certification scheme for indoor built environments during heat waves, Energy and Built Environ (2024), https://doi.org/10.1016/j.enbenv.2024.05.001.
[25] T. Kesik, W. O'brien, A. Ozkan, Toward a standardized framework for thermal resilience modelling and its practical application to futureproofing, Sci. Technol. Built Environ. 28 (2022) 742–756, https://doi.org/10.1080/23744731.2022.2043069.
[26] A.F. Krelling, et al., Defining weather scenarios for simulation-based assessment of thermal resilience of buildings under current and future climates: a case study in Brazil, Sustain. Cities Soc. 107 (2024) 105460, https://doi.org/10.1016/j.scs.2024.105460.
[27] K. Kim, A. Luna-Navarro, J. Ciurlanti, S. Bianchi, A multi-criteria decision support framework for designing seismic and thermal resilient facades, Archit. Struct. Constr. (2024), https://doi.org/10.1007/s44150-024-00116-0.
[28] L. Bertilsson, et al., Urban flood resilience – a multi-criteria index to integrate flood resilience into urban planning, J. Hydrol. 573 (2019) 970–982, https://doi.org/10.1016/j.jhydrol.2018.06.052.
[29] R. Gentile, et al., Scoring, selecting, and developing physical impact models for multi-hazard risk assessment, Int. J. Disaster Risk Reduct. 82 (2022) 103365, https://doi.org/10.1016/j.ijdrr.2022.103365.

[30] Z. Ahmadi, M. Ghasemi, A.M. Khavarian-Garmsir, M. Ahmadi, Integrating flood and earthquake resilience: a framework for assessing urban community resilience against multiple hazards, J. Saf. Sci. Resil. 5 (2024) 330–343, https://doi.org/10.1016/j.jnlssr.2024.05.002.
[31] S. De Angeli, et al., A multi-hazard framework for spatial-temporal impact analysis, Int. J. Disaster Risk Reduct. 73 (2022) 102829, https://doi.org/10.1016/j.ijdrr.2022.102829.
[32] X.W. Zheng, H.N. Li, P. Gardoni, Reliability-based design approach for high-rise buildings subject to earthquakes and strong winds, Eng. Struct. 244 (2021) 112771, https://doi.org/10.1016/j.engstruct.2021.112771.
[33] K. Otárola, L. Iannacone, R. Gentile, C. Galasso, A Markovian Framework to Model life-cycle Consequences of Infrastructure Systems in a multi-hazard Environment, Life-Cycle of Structures and Infrastructure Systems, CRC Press, 2023.
[34] L. Iannacone, K. Otárola, R. Gentile, C. Galasso, Simulating multi-hazard event sets for life cycle consequence analysis, Nat. Hazards Earth Syst. Sci. 24 (2024) 1721–1740, https://doi.org/10.5194/nhess-24-1721-2024.
[35] C. Zhai, Y. Zhao, W. Wen, H. Qin, L. Xie, A novel urban seismic resilience assessment method considering the weighting of post-earthquake loss and recovery time, Int. J. Disaster Risk Reduct. 84 (2023) 103453, https://doi.org/10.1016/j.ijdrr.2022.103453.
[36] C. Ma, Y. Zhao, H. Wang, D. Lu, G. Wang, Development of seismic resilience index and assessing framework of underground frame structures based on economic loss, Soil Dynam. Earthq. Eng. 194 (2025) 109373, https://doi.org/10.1016/j.soildyn.2025.109373.
[37] G.P. Cimellaro, C. Renschler, A.M. Reinhorn, L. Arendt, PEOPLES: a framework for evaluating resilience, J. Struct. Eng. 142 (2016) 4016063, https://doi.org/10.1061/(ASCE)ST.1943-541X.0001514.
[38] S. Monna, Integrated approach for intelligent envelope design: simulation performance of building envelope design strategies and technologies during the early design stage. 1st International Conference on Building Sustainability Assessment, 2014. Porto, Portugal.
[39] S. Bianchi, C. Andriotis, T. Klein, M. Overend, Multi-criteria design methods in façade engineering: state-of-the-art and future trends, Build. Environ. 250 (2024) 111184, https://doi.org/10.1016/j.buildenv.2024.111184.
[40] MULTICARE project, Multi-hazard low-carbon resilient technologies and multi-scale digital services for a future-proof, sustainable & user-centred built environment. https://multicare-project.eu/, 2024.
[41] ANSI/ASHRAE 55, Thermal Environmental Conditions for Human Occupancy, American National Standard, 2023.
[42] W. Ji, et al., Interpretation of standard effective temperature (SET) and explorations on its modification and development, Build. Environ. 210 (2022) 108714, https://doi.org/10.1016/j.buildenv.2021.108714.
[43] A. Gasparrini, et al., Mortality risk attributable to high and low ambient temperature: a multicountry observational study, Lancet 9991 (2015) 369–375, https://doi.org/10.1016/S0140-6736(14)62114-0.
[44] NZSEE, The Seismic Assessment of Existing Building – Technical Guidelines for Engineering Assessments, New Zealand Society of Earthquake Engineering, 2017. Wellington, New Zealand.
[45] Ministero delle Infrastrutture, Linee guida per la classificazione del rischio sismico delle costruzioni, in: A. Allegato (Ed.), Decreto Ministeriale 65 of 07/03/2017, 2017 (in Italian).
[46] F. Jalayer, P. Franchin, P.E. Pinto, A scalar damage measure for seismic reliability analysis of RC frames, Earthq. Eng. Struct. Dynam. 36 (2007) 2059–2079, https://doi.org/10.1002/eqe.704.
[47] ASCE, Prestandard for Performance-based Wind Design, 2019, https://doi.org/10.1061/9780784482186.
[48] M. Francioli, F. Petrini, Performance-based multi-hazard engineering (PB-MH-E): the case of steel buildings under earthquake and wind, Reliab. Eng. Syst. Saf. 251 (2014) 110326, https://doi.org/10.1016/j.ress.2024.110326.
[49] FEMA, Flood Damage - Resistant Materials Requirements, Technical Bulletin, vol. 2, 2008. Washington D.C., USA.
[50] FEMA, HAZUS Hurricane Model, Technical Manual: Hazus 5.1, 2022. Washington D.C., USA.
[51] N. Wang, et al., The seismic resilience-based methodology of regional building function recovery assessment, Soil Dynam. Earthq. Eng. 180 (2024) 108601, https://doi.org/10.1016/j.soildyn.2024.108601.
[52] P. Kourehpaz, C. Molina Hutt, C. Galasso, Improving recovery time consequence models in regional seismic risk assessment by leveraging high-fidelity building-specific recovery simulations, Earthq. Spectra 0 (2025), https://doi.org/10.1177/87552930251344981.
[53] N. Ismail, D. Ouahrani, A. Al Touma, Quantifying thermal resilience of office buildings during power outages: development of a simplified model metric and validation through experimentation, J. Build. Eng. 72 (2023), https://doi.org/10.1016/j.jobe.2023.106564.
[54] FEMA, HAZUS Earthquake Model Technical Manual: Hazus 6.1, 2024. Washington D.C., USA.
[55] FEMA, HAZUS Flood Model Technical Manual: Hazus 6.1, 2024. Washington D.C., USA.
[56] ASCE, Flood Resistant Design and Construction, ASCE/SEI Standard, Virginia, USA, 2015, https://doi.org/10.1061/9780784485781, 24-14.
[57] P. Franchin, F. Noto, Reliability-based partial factors for seismic design and assessment consistent with second-generation Eurocode 8, Earthq. Eng. Struct. Dynam. 52 (2023) 4026–4047, https://doi.org/10.1002/eqe.3840.
[58] T.L. Saaty, The Analytic Hierarchy Process, McGraw-Hill, 1980.
[59] M. Duarte, N. Almeida, M.J. Falcão, S.M.H.S. Rezvani, Resilience rating system for buildings against natural hazards. 15th WCEAM Proceedings, WCEAM 2021, Lecture Notes in Mechanical Engineering, Springer, 2022, https://doi.org/10.1007/978-3-030-96794-9_6.
[60] S. Bianchi, Integrating resilience in the multi-hazard sustainable design of buildings, Dis. Prev. Res. 2 (2023) 14, https://doi.org/10.20517/dpr.2023.16.
[61] C.L. Hwang, K. Yoon, Multi Attribute Decision Making: Methods and Applications: a State of the Art Survey, Springer, 1981.
[62] D. Diakoulaki, G. Mavrotas, L. Papayannakis, Determining objective weights in multiple criteria problems: the CRITIC method, Comput. Oper. Res. 22 (1995) 7, https://doi.org/10.1016/0305-0548(94)00059-H.
[63] A.E. Zaghi, J.E. Padgett, M. Bruneau, M. Barbato, Y. Li, J. Mitrani-Reiser, A. McBride, Establishing common nomenclature, characterizing the problem, and identifying future opportunities in multihazard design, J. Struct. Eng. 142 (2016) H2516001, https://doi.org/10.1061/(ASCE)ST.1943-541X.0001586.
[64] S. Hassoun, s. Fundamentals of Artificial Neural Network, 1995.
[65] F. de Vries, Hittebestendig Wonen Met Een Lage Energievraag, Amsterdam University of Applied Sciences, 2023.
[66] KNMI, National climate scenarios 2023 for the Netherlands KNMI number: WR-23-02. knmi.nl/kennis-en-datacentrum/publicatie/knmi-national-climate-scenarios-2023-for-the-netherlands, 2023.
[67] Global Historical Climatology Network - Daily (GHCN-Daily), Version 3. National Centers for Environmental Information (NCEI). https://www.ncei.noaa.gov/access/search/data-search/daily-summaries?pageNum=1 (accessed 10 March 2025).
[68] S.E. Perkins, L.V. Alexander, On the measurement of heat waves, J. Clim. 26 (2013) 4500–4517, https://doi.org/10.1175/JCLI-D-12-00383.1.
[69] US Department of Energy's Building Technologies Office, Energyplus, DOE-BTO, 2001.
[70] M. Dang, A. van den Dobbelsteen, P. Voskuilen, A parametric modelling approach for energy retrofitting heritage buildings: the case of Amsterdam City Centre, Energies 17 (2024) 994, https://doi.org/10.3390/en17050994.
[71] USGBC, IPpc100, Passive Survivability and Back-up Power During Disruptions, 2019.
[72] I.X. Bijlage, Omgevingsregeling van 21 November 2019, Minister voor Milieu en Wonen, Staatssecretaris van Defensie, Minister van Economische Zaken en Klimaat, Minister van Infrastructuur en Waterstaat, Minister van Landbouw, Natuur en Voedselkwaliteit, Minister van Onderwijs, Cultuur en Wetenschap (in Dutch), https://wetten.overheid.nl/BWBR0045528/2024-07-01/0. (Accessed 10 March 2025).
[73] Osservatorio Nazionale CittàClima. https://cittaclima.it/. (Accessed 10 March 2025).
[74] S. Pampanin, A step-change for seismic risk reduction, (towards a) national plan for the integrated seismic-energetic rehabilitation of the building stock, Struct. Magazine (2023), https://doi.org/10.12917/STRU242.15.
[75] Weather Forecast Api, Open-Meteo. https://open-meteo.com/en/docs. (Accessed 10 March 2025).
[76] G.M. Calvi, L. Sousa, C. Ruggeri, Energy efficiency and seismic resilience: a common approach, in: Multi-Hazard Approaches to Civil Infrastructure Engineering, vol. 9, Springer Intern. Pub., 2016, pp. 165–208, https://doi.org/10.1007/978-3-319-29713-2.

[77] I. Iervolino, A. Spillatura, P. Bazzurro, Seismic reliability of code-conforming Italian buildings, J. Earthq. Eng. 22 (2018) 5–27, https://doi.org/10.1080/13632469.2018.1540372.
[78] C.A. Cornell, H. Krawinkler, Progress and challenges in seismic performance assessment, PEER Cent. News 3 (2000) 1–3. berkeley.edu/news/2000spring/performance.html.
[79] M. Stucchi, et al., Seismic hazard assessment (2003–2009) for the Italian building code, Bull. Seismol. Soc. Am. 101 (2011) 1885–1911, https://doi.org/10.1785/0120100130.
[80] Ministero delle Infrastrutture, Aggiornamento delle Norme Tecniche per le Costruzioni, Supplemento Ordinario N 8 Alle G.U. No 42 Del 20/02/2018, 2018. Rome, Italy (in Italian).
[81] K. Aljawhari, R. Gentile, C. Galasso, Simulation-based consequence models of seismic direct loss and repair time for archetype reinforced concrete frames, J. Build. Eng. 84 (2024) 108149, https://doi.org/10.1016/j.jobe.2023.108149.
[82] Ministerial Decree No 515 of 3 June 1981 (DM 03/6/1981), Classificazione «A Bassa Sismicità» S = 6 Del Territorio Dei Comuni Delle Regioni Basilicata, Campania E Puglia E Classificazione Sismica S = 9 Del Territorio Del Comune Di S. Maria La Carità', Official Gazzette, 1981. Italy, General Series No 162(in Italian).
[83] CNR, Istruzioni per la Valutazione Delle Azioni E Degli Effetti Del Vento Sulle Costruzioni, CNR-DT 207 R1/2018, 2019 (in Italian).
[84] B. Feuerstein, et al., Towards an improved wind speed scale and damage description adapted for Central Europe, Atmos. Res. 100 (2011) 547–564, https://doi.org/10.1016/j.atmosres.2010.12.026.
[85] E.E. Koks, T. Haer, A high-resolution wind damage model for Europe, Sci. Rep. 10 (2020) 6866, https://doi.org/10.1038/s41598-020-63580-w.
[86] C.C. Sampson, et al., A high-resolution global flood hazard model, Water Resour. Res. 51 (2015) 7358–7381, https://doi.org/10.1002/2015WR016954.
[87] Gemeente Amsterdam, the Heat Program. https://denkmee.amsterdam.nl/heatprogram/, 2024.
[88] A. Arup, Universal taxonomy for natural hazard and climate risk and resilience assessments. arup.com/insights/a-universal-taxonomy-for-natural-hazard-and-climate-risk-and-resilience-assessments/, 2024.
[89] L. Pedone, S. Bianchi, S. Giovinazzi, S. Pampanin, A framework and tool for knowledge-based seismic risk assessment of school buildings: slama-school, Sustainability 14 (2022) 9982, https://doi.org/10.3390/su14169982.

Update

International Journal of Disaster Risk Reduction
Volume 139, Issue , 1 June 2026, Page

DOI: https://doi.org/10.1016/j.ijdrr.2026.106129

International Journal of Disaster Risk Reduction 139 (2026) 106129

Contents lists available at ScienceDirect

International Journal of Disaster Risk Reduction

journal homepage: www.elsevier.com/locate/ijdrr

Corrigendum

Corrigendum to 'Resilience readiness levels for buildings: Establishing multi-hazard resilience metrics and rating systems' [Int. J. Disaster Risk Reduct. 128 (2025) 105746]

Simona Bianchi [a,*], Michele Matteoni [b], Kyujin Kim [a], Anna Maria Koniari [a], Kyra Koning [c], Romulus Costache [d], Nicu Ciobotaru [d], Alessandra Luna-Navarro [a], Zhikai Peng [a,c], Jonathan Ciurlanti [e], Hamidreza Shahriari [f], Divyae Mittal [f], Evdokia Stavridou [f], Anna Silva [a,c], Michele Palmieri [e], Stefano Pampanin [b], Francesco Petrini [b], Mauro Overend [a]

[a] Delft University of Technology, 2628 BL, Delft, the Netherlands
[b] Sapienza University of Rome, 00184, Rome, Italy
[c] Amsterdam Institute for Advanced Metropolitan Solutions, 1018 JA, Amsterdam, the Netherlands
[d] Transilvania University of Brasov, 500123, Brasov, Romania
[e] Arup, 1043 CA, Amsterdam, the Netherlands
[f] OMRT, 1013 AC, Amsterdam, the Netherlands

The authors wish to replace the flood hazard map in Fig. 11a with an updated map for the Acerra region. The legend has been revised to display only the minimum and maximum flood depth values.

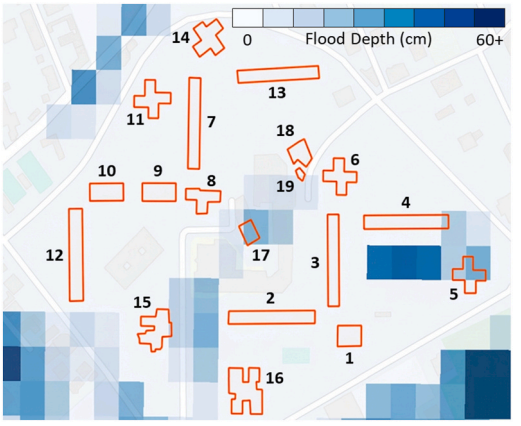

Fig. 11. (a) Flood hazard map for the Acerra region (Pluvial flooding - RCP 8.5 for year 2050, 50th Percentile - 1000 years return period) overlayed on the case study buildings (highlighted in orange).

DOI of original article: https://doi.org/10.1016/j.ijdrr.2025.105746.
* Corresponding author.
E-mail address: s.bianchi@tudelft.nl (S. Bianchi).

https://doi.org/10.1016/j.ijdrr.2026.106129

Available online 10 April 2026